

Water-Based Lubricants for Electric Vehicle
Transmission Applications: Properties,
Tribological Performance and Efficiency

Mushfiq Hasan

Machine Elements

Water-Based Lubricants for Electric Vehicle Transmission Applications: Properties, Tribological Performance, and Efficiency

Mushfiq Hasan

Supervisors:

Prof. Roland Larsson

Associate Prof. Marcus Björling

Division of Machine Elements

Department of Engineering Sciences and Mathematics

Luleå University of Technology, Sweden



Copyright ©Mushfiq Hasan (2026).

This document is freely available at:

www.ltu.se

or by contacting Mushfiq Hasan:

mushfiqhasan09@gmail.com

This document may be freely distributed in its original form when including the current author's name. None of the content may be changed or excluded without permission from the author.

Identifiers

URN: urn:nbn:se:ltu:diva-116500

ISBN: 978-91-8048-995-9 (print)

ISBN: 978-91-8048-996-6 (electronic)

OAI: oai:DiVA.org:ltu-116500

DiVA, id: [diva2:2040299](#)

Luleå, 2026

To everyone whose kind support helped turn obstacles into milestones!

PREFACE

This project was financially supported by the Swedish Automotive Research Initiative (FFI) and the Swedish Energy Agency (Grant No. 51939–1 and 2020–024802), which is gratefully acknowledged. I also sincerely appreciate the contributions of all the lubricant suppliers, without whom this work would not have been possible.

My sincere gratitude goes to my supervisors, Roland Larsson and Marcus Björling, for their continuous guidance and support. I am especially grateful to Roland for his kind mentorship and for allowing me the independence to develop as a researcher. Over the past four years, this freedom has enabled me to gain the confidence to explore research challenges beyond my primary area of expertise. His encouragement and guidance helped me remain focused during tough times. I am equally grateful to Marcus for his constant support whenever I encountered challenges in the laboratory or during the writing process. Our discussions, often spontaneous in his office or over Teams, were always insightful and helped me to speed up my work before deadlines. I deeply appreciate the time, knowledge, and experience that both of my supervisors generously shared with me throughout this journey.

I would also like to thank our project partners, SKF and Volvo Cars, for their collaboration and support. I am particularly grateful to Christine Matta for generously sharing her expertise and for giving me the opportunity to work in the SKF RTD laboratory. I also extend my gratitude to Frank Berens and Kenred Stadler for their valuable insights during project meetings. Special thanks go to Ralph Meeuwenoord for his support during my visit to SKF, particularly with the WAM test setup, and to Ugo Jantel from Volvo Cars for his continuous support through meetings, emails, and conference participation. I would also like to thank Johan Stjärnesund for sharing his expertise in testing, and Robin Elo for supporting with characterisation. In addition, I acknowledge Luiz Pereira, Tommy Brandt, and Robert Johansson for their contributions to the project during its early stages.

I am greatly indebted to the Machine Elements division at Luleå University of Technology for providing a welcoming and supportive research environment. I am especially thankful to Pär Marklund, Jens Hardell, Yijun Shi, Leonardo Pelcastre, and Erik Nyberg for their valuable discussions and support. I also thank Anders Pettersson for serving as the examiner at my mid-seminar and for providing constructive feedback. Special thanks go to Nazanin Emami, who first introduced me to Luleå and the Machine Elements division during my master's studies. I am also grateful to Markus Söderfjäll for his support in the Tribolab.

I feel fortunate to have such wonderful colleagues who provided both professional and emotional support during challenging times. I thank Gabriel, Nayan, Lisa, Myrna, Daria, John, Gustav, Ben, Dilesh, Zhipeng, Idiris, and Lars for their friendship and encouragement. I am also grateful to Lucas and Maksim for their help with access to the polymer laboratory. Special thanks go to Pontus and Jun Chen for their consistent support in the laboratory whenever I needed assistance. I also thank Deepak, Vahid and Jun Zhao for the many

stimulating discussions on lubricants, EHL, and simulation. I would also like to acknowledge my peers across LTU for contributing to a memorable and enjoyable PhD experience. I will always cherish the moments and memories we shared.

A special acknowledgement goes to my former supervisors, especially to Dewan Hasan Ahmed, who introduced me to research and inspired me to pursue a PhD. I would also like to thank Tanvir Iqbal for his guidance since childhood. I am grateful to my friend Juan Guillermo for our many discussions on tribology, food, and life. I also thank all my friends including Farhan, Sharif, and Sunny for their unconditional friendship over the years.

I have also been fortunate to meet Wasim Choudhury and Asma Ahmed, who always took care of me and provided the warmth of home in Luleå. I would also like to thank Mashreki Sami and Rokshan Ara for their constant support whenever I needed help. I am deeply grateful to my fellow countrymen in Luleå for their social engagement and support.

Finally, I would like to express my deepest gratitude to my family. I thank my parents, Sajedul Hasan and Shamim Ara, for their lifelong encouragement, love, and blessings. Without their support, I would not be where I am today. I also thank Raka and Arafat for their affection and support. My heartfelt thanks go to my wife, Shama, who joined me during the later stage of this journey and shared it with patience and love.

Med vänliga hälsningar,

Mushfiq Hasan

March 2026

ABSTRACT

Water-based lubricants (WBLs) are emerging as promising alternatives to conventional oil-based lubricants in electric vehicle (EV) transmission systems, driven by increasing demands for energy efficiency, sustainability, thermal management, and environmental compatibility. Original equipment manufacturers (OEMs) and researchers are striving to minimise frictional, thermal, and power losses in EV gearboxes to maximise driving range and system durability, and WBLs have the potential to meet this demand. Moreover, WBLs offer flexibility in viscosity tuning, higher specific heat capacity, and superior heat transfer capability compared with oil-based lubricants. These characteristics create opportunities to improve cooling performance and support the development of a single e-fluid concept. However, their successful implementation requires a comprehensive understanding of film formation, friction, and wear behaviour, system-level efficiency, and material compatibility.

This thesis investigates the feasibility of WBLs for EV transmissions through a series of interconnected studies. It begins with the characterisation of elastohydrodynamic (EHL) film formation and pressure-viscosity relationships, revealing the distinctive film-forming behaviour of WBLs. The effects of water content and evaporation sensitivity on the pressure-viscosity coefficient are examined, and the applicability of classical predictive models, including the Hamrock–Dowson equation, is reassessed. Friction and wear analyses demonstrate that fully formulated WBLs can achieve near-superlubricity with minimal shear heating, facilitated by robust surface-additive interactions under rolling/sliding contact. These laboratory findings are validated through full-scale EV gearbox testing, where WBLs reduce power losses and thermal load, improving overall gearbox peak efficiency by approximately 1.95%, 1.84%, and 1.63% at 20 °C, 40 °C, and 60 °C, respectively. Finally, durability is evaluated via tribocorrosion analysis of bearing steel, highlighting the synergistic interaction between mechanical and chemical wear in aqueous environments.

Overall, this work positions WBLs as a promising high-efficiency and environmentally friendly e-fluid for future sustainable transportation, provided that challenges related to water loss and wear are effectively addressed through advanced formulation and system design.

APPENDED PAPERS

Paper A **Hasan, M.**, Björling, M., Matta, C., Meeuwenoord, R., Jantel, U., & Larsson, R. (2025). An investigation of film formation and pressure-viscosity relationship of water-based lubricants in elastohydrodynamic contacts. *Tribology International*, 208, 110654.

Paper B **Hasan, M.**, Björling, M., Elo, R., Matta, C., Jantel, U., & Larsson, R. (2026). Friction and wear behaviour of fully formulated water-based lubricants under rolling/sliding contacts. *Tribology International*, 111669.

Paper C **Hasan, M.**, Björling, M., Jantel, U., Stjärnesund, J., Matta, C., & Larsson, R. (2026). Drag loss and efficiency analysis of an electric vehicle gearbox using water-based lubricants. *Submitted in Results in Engineering*.

Paper D **Hasan, M.**, Björling, M., Johansson, P., & Larsson, R. (2026). Tribocorrosion behaviour of bearing steel in glycerol-based solutions. *(To be communicated)*

Hasan, M. Contributions:

Conceptualisation, Methodology, Investigation, Formal analysis, Data curation, Visualisation, Validation, Writing—original draft.

ADDITIONAL PAPERS

- Paper A** Pradhan, A., Müser, M. H., Miller, N., Abdelnabe, J. P., Afferrante, L., Albertini, D., ... & Zhang, X. (2025). The surface-topography challenge: A multi-laboratory benchmark study to advance the characterization of topography. *Tribology letters*, 73(3), 110.
- Paper B** Okhiria, P., Björling, M., Johansson, P., Hasan, M., Larsson, R., & Shi, Y. (2024). Tribological Performance of Glycerol-Based Hydraulic Fluid Under Low-Temperature Conditions. *Lubricants*, 12(12), 430.
- Paper C** Hasan, M., Mohammed, O. D., Kolar, C., Björling, M., & Larsson, R. (2022). Study of wear and micropitting in rolling/sliding contacts operating under boundary lubrication conditions. *Procedia Structural Integrity*, 42, 1169-1176.

CONFERENCE CONTRIBUTIONS

Hasan, M., Björling, M., & Larsson, R.

Investigation of running-in behaviour under glycerol and oil-based lubrication

Nordic Symposium on Tribology (NordTrib), 14-17 June 2022, Ålesund, Norway.

Oral presentation/accepted abstract

Hasan, M., Björling, M., & Larsson, R.

A comparative tribological study between sustainable and fossil-based lubrication

1st International Conference on Tribology and Sustainable Lubrication, 18-19 April 2023, Düsseldorf, Germany.

Oral presentation/accepted abstract/Proceedings

Hasan, M., Björling, M., Matta, C., Jantel, U., & Larsson, R.

An Investigation of Film Formation and Pressure Viscosity Relation of Water-Based Lubricants.

78th STLE Annual Meeting & Exhibition, Minneapolis, USA. 19-23 May 2024.

Oral presentation/accepted abstract

Hasan, M., Björling, M., Matta, C., Jantel, U., & Larsson, R.

Exploring the Potential of Water-Based Lubricants for Electric Vehicle Transmission Application.

2025 STLE Tribology & Lubrication for E-Mobility Conference, Detroit, Michigan. 19-21 November 2025.

Oral presentation/accepted abstract

NOMENCLATURE

η	Viscosity at any given pressure (Pa s)
η_0	Viscosity at atmospheric pressure (Pa s)
α	Pressure-viscosity coefficient (Pa ⁻¹)
α_0	Conventional pressure-viscosity coefficient (Pa ⁻¹)
α^*	Reciprocal asymptotic isoviscous pressure coefficient (Pa ⁻¹)
α_{film}	Universal pressure-viscosity coefficient (Pa ⁻¹)
<i>EHL</i>	Elastohydrodynamic Lubrication
<i>PAG</i>	Polyalkylene Glycol
<i>PEG</i>	Polyethylene Glycol
<i>DEG</i>	Diethylene glycol
<i>WBL</i>	Water-Based Lubricants
<i>SRR</i>	Slide to Roll ratio
h_c	Central film thickness (m)
H_{RI}	Dimensionless central film thickness for the rigid isoviscous condition
H_{RP}	Dimensionless central film thickness for the rigid piezoviscous condition
H_{EI}	Dimensionless central film thickness for the elastic-isoviscous condition
H_{EP}	Dimensionless central film thickness for the elastic-piezoviscous condition
L	Dimensionless material parameter (Moes)= $G(2U)^{0.25}$
M	Dimensionless load parameter (Moes)= $W/(2U)^{0.75}$
U	Dimensionless speed parameter (Hamrock and Dowson) = $\eta u_e/(E'R_x)$
W	Dimensionless load parameter (Hamrock and Dowson) = $w/(E'R_x^2)$
G	Dimensionless material parameter (Hamrock and Dowson) = $\alpha E'$
u_e	Entrainment speed (m/s)

w	Load (N)
E'	Reduced modulus of elasticity (Pa)
R_x	Reduced radii of curvature in the entrainment direction (m)
R_y	Reduced radii of curvature perpendicular to the entrainment direction (m)
D	Ratio of reduced radius of curvature
ρ	Density (kg/m^3)
C	Calibration factor, $C = C_0 + C_1T + C_2T_2$; $T =$ temperature in $^\circ\text{C}$
t	Time required for a change of LVDT-conditioned output of 1000 mV (S)
a_v	Thermal expansivity defined for volume linear with temperature (K^{-1})
β_k	Temperature coefficient of K_0 (K^{-1})
K_0	Isothermal bulk modulus at ($P = 0$) (Pa)
K'_0	Pressure rate of change of isothermal bulk modulus at ($P = 0$)
K_{00}	K_0 at zero absolute temperature (Pa)
V	Volume at T and P (m^3)
V_R	Volume at reference state, T_R , ($P = 0$) (m^3)
V_0	Volume at $P = 0$ (m^3)
T	Temperature (K)
T_R	Reference temperature (K)
N	Number of units
H_C	Dimensionless central film thickness
n	Refractive index
n_0	Refractive index at atmospheric pressure
g^E	Dimensionless elasticity parameter (Moes) = $W^{\frac{8}{3}}/U^2$
g^V	Dimensionless viscosity parameter (Moes) = GW^3/U^2

CONTENTS

PART A. COMPREHENSIVE SUMMARY

1	Introduction	3
1.1	Background.....	3
1.2	Definition of water-based lubricants.....	4
1.3	Importance of water-based lubricants in EV	4
1.4	Thesis outline	6
2	Frame of Reference	7
2.1	EHL lubricated contact.....	7
2.2	Lubricant rheology	8
2.2.1	Shear behaviour of lubricants.....	8
2.2.2	Temperature-viscosity relationship.....	9
2.2.3	Pressure-viscosity relationship	10
2.2.4	Equation of state.....	11
2.2.5	Pressure-viscosity coefficient definitions	12
2.3	Isothermal EHL film thickness equations.....	14
2.4	EHL regimes	16
2.5	Friction in rolling/sliding contact.....	17
2.6	Superlubricity in rolling/sliding contacts	19
2.7	Failure modes	20
2.8	Gearbox efficiency and power loss	22
3	Background & Research Gap	25
3.1	State of the art	25
3.2	Identified research gaps	30
3.3	Research questions	32
4	Experimental Methodology.....	33
4.1	Candidate lubricants	33
4.2	Tribotesting: ball on disc tribometer.....	35
4.2.1	Stribeck and traction measurements (WAM).....	35
4.2.2	EHL film thickness measurements (WAM)	35

4.2.3	Wear and tribofilm studies (MTM2)	36
4.3	Pressure-viscosity coefficient determination.....	37
4.3.1	Film thickness derived pressure-viscosity coefficient	37
4.3.2	Viscometer derived pressure-viscosity coefficient.....	38
4.4	Drag loss and efficiency tests	39
4.5	Tribocorrosion test	41
4.6	Surface characterisation	42
4.7	Fluid characterisation	43
5	Results.....	45
5.1	EHL film formation and pressure-viscosity relationship.....	45
5.2	Analysis of frictional behaviour	52
5.3	Wear evolution and characterisation.....	55
5.4	Tribocorrosion behaviour	58
5.5	Gearbox drag losses and efficiency.....	60
5.6	Influence of test setup on WBLs evaporation.....	62
6	Concluding Remarks	65
7	Future Perspectives	71
	Paper A	85
	Paper B	101
	Paper C.....	115
	Paper D.....	141

PART A. COMPREHENSIVE SUMMARY

1 Introduction

1.1 Background

Over the past decades, sustainability and carbon neutrality have become key drivers of research across many disciplines, including tribology. Lubrication plays a vital role in rotating components by reducing friction, which in turn lowers energy consumption and CO₂ emissions. However, the environmental impact of the lubricant itself must also be considered, as it can affect both ecosystems and human health.

State-of-the-art lubricants are predominantly petroleum-based and rely on high-performance additive packages containing sulphur, zinc, ash-forming compounds, and other chemically active elements [1]. While these lubricants have been developed over centuries and are capable of withstanding extreme operating conditions, increasing environmental regulations are now pushing OEMs and researchers to seek alternatives that reduce dependence on fossil resources and overall energy consumption. At present, there is no fully fossil-free lubricant that can match the mechanical performance of conventional mineral oil-based products. Bio-based lubricants, such as those derived from vegetable oils, have been proposed as alternatives; however, their long-term viability is limited, as many natural oils are also important dietary resources.

Water-based or water-soluble lubricants (WBLs) have gained increasing attention in recent years as a potential alternative to mineral-based lubricants. They offer promising opportunities for greener solutions in applications such as marine systems, hydraulics, metalworking, and even electric vehicle transmissions. However, the lubrication mechanisms of WBLs differ significantly from those of conventional oils, making it challenging to directly apply existing formulation knowledge. In addition, developing environmentally friendly additive packages that meet demanding performance requirements remains a major research challenge. This PhD project, therefore, focuses on a detailed tribological investigation of WBLs, with particular emphasis on their application in electric vehicle transmissions.

The project is strongly motivated by its potential contribution to the Sustainable Development Goals (SDGs). Its primary impact lies in identifying environmentally friendly alternatives to conventional lubricants that can improve electric vehicle efficiency, thereby directly supporting several SDGs, including Goal 7 (Affordable and

Clean Energy), Goal 9 (Industry, Innovation, and Infrastructure), and Goal 11 (Sustainable Cities and Communities).

1.2 Definition of water-based lubricants

Water-based or water-soluble lubricants are formulations in which water is used either as the primary base fluid or as a functional component, depending on the application and formulation strategy. Pure water alone is a poor lubricant for extreme operating conditions due to its very low viscosity and weak pressure-viscosity response, which limits its ability to form a protective lubricating film [2]. To overcome these limitations, water is combined with various water-soluble compounds that act as base stocks or additives to enhance friction reduction and film-forming capability. Commonly used components include polyalkylene glycols (PAG), polyethylene glycols (PEG), glycerol, esters, and certain ionic liquids [3]. Depending on the intended application, water-based lubricants typically contain a significant proportion of water, generally ranging from about 10% to 70%. All associated components are selected to be water-soluble, ideally non-toxic, and biodegradable to support the sustainability objectives of water-based lubrication systems. In this thesis, lubricants containing a significant proportion of water together with water-soluble compounds are referred to as water-based lubricants. Some example formulations of WBL are stated below:

- a. 45 wt.% water + 20 wt.% propylene glycol + 25 wt.% polyethylene glycol + additives [4].
- b. 80 wt.% water + 20 wt.% polymer + additives (AW, EP) [5].
- c. 95 wt.% Glycerol + 5 wt.% water [6].

1.3 Importance of water-based lubricants in EV

An electric drive unit (EDU) is the propulsion system of a battery electric vehicle (BEV). Unlike internal combustion vehicles, which use separate components such as engine, transmission, and engine control unit, modern electric vehicles employ a compact, integrated propulsion module [7]. The EDU combines an electric motor, power electronics (inverter and controller), and a gearbox or differential into a single unit. The electric motor converts electrical energy into mechanical torque, the power electronics regulate current and control motor speed, and the gearbox adapts the motor's high-speed rotation into usable torque at the wheels.

Even though an electric vehicle already has a motor, a gearbox is still required to match the motor's characteristics to the vehicle's driving needs. The gearbox multiplies torque at low vehicle speeds and enables the motor to operate closer to its optimal efficiency range under varying driving conditions. Most EVs use a simple single-speed reduction gearbox, as shown in Figure 1, which is far simpler than the multi-speed transmissions used in internal combustion vehicles. A single-speed gearbox in an electric

vehicle is a two-stage reduction unit that connects the high-speed electric motor to the wheels. It primarily consists of an input shaft connected to the motor, a fixed reduction gear set that lowers speed and increases torque, and an output shaft that delivers power to the wheels. The reducer also houses the differential, which splits torque between the drive shafts. Typical reduction ratios commonly found include 8.27:1, 11.45:1, and 12.25:1. For higher-end and high-performance vehicles, some OEMs are adopting multi-speed gearboxes to improve acceleration and efficiency at high speeds. One of the earliest attempts to use a multi-speed gearbox in an electric vehicle was in the first-generation Tesla Roadster [8].

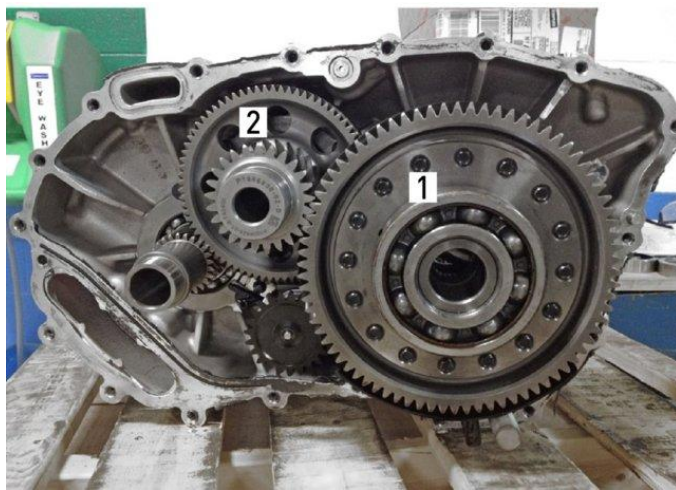


Figure 1: Tesla Model S transmission showing the output ring gear (1) and the intermediate gear (2). Source: [9]

Even though modern EV gearboxes eliminate clutches and multiple gear stages, lubrication is still essential. The lubricant is needed to reduce friction, wear and provide adequate film thickness between contacting surfaces, and it also helps transport heat away from heavily loaded components to ensure reliable operation. There is a higher cooling demand than before to dissipate heat from battery storage and other electrical components to maintain efficiency and longevity. OEMs are constantly looking for a single fluid that can fulfil the needs of coolant and transmission fluid. In this case, the fluid needs to be designed in a balanced way from the tribological, thermal and efficiency points of view. It is quite a challenging task for conventional fluids to meet all the criteria while keeping the environment and sustainability impact in mind.

Overall, water-based lubricants present a promising solution for meeting the combined lubrication and cooling demands of electric vehicle drivetrains in an

environmentally sustainable way. The high heat capacity of water makes it particularly attractive for effective thermal management, which is critical in EV applications. When blended with functional additives, WBLs can also provide improved friction, wear resistance and load carrying capacity. Nevertheless, further optimisation of formulations and comprehensive tribological studies are still required to enable reliable and widespread industrial adoption.

1.4 Thesis outline

The PhD thesis is structured as follows.

- Chapter 2 provides background information on the lubrication of rolling/sliding contacts, common failure modes, and transmission efficiency, including mechanisms of power loss.
- Chapter 3 presents a comprehensive literature review and discusses recent developments in water-based lubricants, with a focus on rolling and sliding contact applications; the research gaps and objectives of the thesis are also defined in this chapter.
- Chapter 4 describes the candidate lubricant formulations, their physicochemical properties, the experimental test rigs, testing methodologies, and post-test characterisation techniques used in this study.
- Chapter 5 presents and discusses the experimental results, with subsections addressing the different research objectives investigated in the thesis.
- Chapter 6 summarises the main conclusions and highlights the outcomes based on research questions.
- Chapter 7 outlines the recommendations and directions for future work.

2 Frame of Reference

Chapter 2 provides the theoretical background and fundamental concepts relevant to this thesis.

2.1 EHL lubricated contact

Elastohydrodynamic lubrication (EHL) occurs in heavily loaded, non-conformal contacts such as gears, rolling element bearings, and cam-follower systems. In these contacts, the interacting surfaces meet over a very small area, producing extremely high contact pressures, typically in the range of 0.5–4 GPa [10]. Under such conditions, classical hydrodynamic lubrication theory is insufficient because both the elastic deformation of the contacting bodies and the pressure-dependent behaviour of the lubricant become significant.

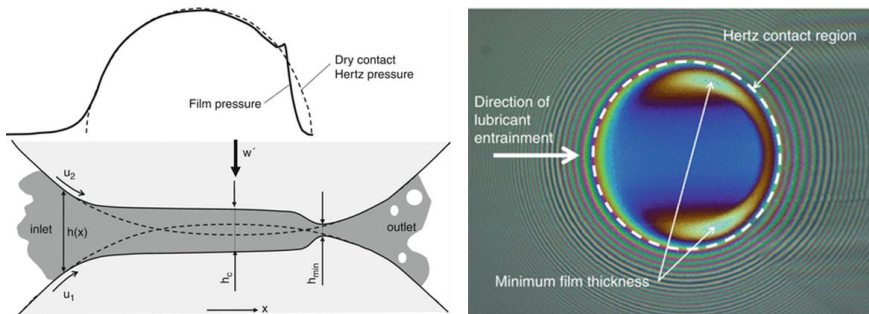


Figure 2: Typical film thickness profile for an EHL contact and corresponding interference pattern representing film thickness in EHL point contact [11].

In an EHL contact, lubricant is entrained into the converging gap formed by the relative motion of the surfaces. As the lubricant enters the contact zone, the pressure rises sharply, causing a dramatic increase in lubricant viscosity due to the piezoviscous effect. Simultaneously, the high pressure elastically deforms the surfaces, increasing the contact area. The combined effect allows the formation of a continuous lubricant film,

despite the extremely small nominal film thickness, which typically lies in the nanometer to micrometer range.

The resulting EHL film consists of two characteristic regions as depicted in Figure 2. Firstly, the central film thickness is nearly constant across the middle of the contact. Secondly, a minimum film thickness is located near the outlet of the contact, where a constriction forms due to flow continuity requirements. Film formation in EHL is primarily governed by conditions in the inlet zone, where lubricant entrainment occurs. Importantly, the pressure and material properties within the Hertzian contact zone have little influence on the final film thickness. Instead, parameters such as entrainment speed, lubricant viscosity at inlet temperature, pressure–viscosity response, and effective contact geometry dominate film formation [10].

2.2 Lubricant rheology

Lubricant rheology describes the relationship between shear stress, shear strain rate, pressure, and temperature within the lubricant film. In EHL contacts, rheological behaviour is crucial because lubricant properties vary significantly across the contact, especially under high pressure and shear conditions. Lubricants may behave as Newtonian or non-Newtonian fluids depending on shear rates and pressure. Another important rheological phenomenon in EHL is the existence of a limiting shear stress. Beyond a certain shear rate, the lubricant can no longer support increasing shear stress, and the stress approaches an asymptotic maximum value. This behaviour significantly influences traction and friction in rolling/sliding contacts. Rheological properties relevant to EHL can be summarised as follows:

- Low-shear viscosity at inlet conditions (important for film thickness)
- Pressure–viscosity dependence (lubricant behaviour under pressure)
- High–pressure shear response (governing friction)

Thus, lubricant rheology plays a dual role: it controls film thickness through inlet behaviour and friction through high–pressure shear behaviour within the contact. Some aspects of lubricant rheology are described in the following subsections.

2.2.1 Shear behaviour of lubricants

Lubricants may be classified as Newtonian or non-Newtonian based on their rheological response to shear. A Newtonian fluid is one in which the shear stress is directly proportional to the shear rate, and the viscosity remains constant regardless of the applied shear conditions. Mineral oils and base lubricants behave as Newtonian fluids under moderate operating conditions, such as low shear rates and temperatures. In these fluids, resistance to flow is governed solely by viscosity, which is independent of shear rate. The flow behaviour of Newtonian lubricants is described by Newton’s law of viscosity, given by:

$$\tau = \mu \frac{du}{dy} \quad (1)$$

where τ is the shear stress, μ is the dynamic viscosity, and $\frac{du}{dy}$ is the shear rate.

In contrast, a non-Newtonian fluid is characterised by a viscosity that varies with shear rate, time, or both. In EHL contacts, the lubricant is subjected to very high pressures and shear rates, particularly in the Hertzian zone. Under these conditions, lubricants often exhibit non-Newtonian behaviour, most notably shear thinning, where apparent viscosity decreases with increasing shear rate [12]. Many modern lubricants, particularly those formulated with polymeric additives such as viscosity index improvers, exhibit non-Newtonian behaviour under high shear conditions. Common non-Newtonian behaviours observed in lubricants include shear-thinning (pseudoplastic behaviour), where viscosity decreases with increasing shear rate; shear-thickening (dilatant behaviour), where viscosity increases with shear rate [12].

2.2.2 Temperature-viscosity relationship

Viscosity decreases with increasing temperature, strongly influencing friction and film thickness in EHL contacts. The sensitivity of a lubricant's viscosity to temperature is often characterised by the viscosity index (VI). A high VI indicates relatively small viscosity changes with temperature, while a low VI corresponds to strong temperature dependence. High-VI lubricants are generally preferred in EHL applications to maintain stable film thickness across a wide operating temperature range.

Another commonly used measure is the temperature-viscosity coefficient, β , which quantifies the rate at which viscosity changes with temperature [13]. This coefficient depends on both temperature and pressure. In general, β increases with pressure, except under conditions of low pressure combined with high temperature. A widely used empirical model to describe the temperature dependence of viscosity in EHL is the Vogel–Tammann–Fulcher (VTF) equation:

$$\eta = \eta_{\infty} \exp\left(\frac{D_F T_{\infty}}{T - T_{\infty}}\right) \quad (2)$$

where μ is the dynamic viscosity, μ_{∞} is the viscosity extrapolated to infinite temperature, D_F is the fragility parameter, and T_{∞} is the Vogel temperature at which viscosity diverges. These parameters are lubricant-specific and are discussed further in the context of rheological modelling. From the VTF formulation, the temperature-viscosity coefficient is given by:

$$\beta = \frac{D_F T_{\infty}}{(T - T_{\infty})^2} \quad (3)$$

This expression highlights the strong non-linear dependence of viscosity on temperature, particularly as the operating temperature approaches T_∞ .

2.2.3 Pressure-viscosity relationship

The pressure-viscosity relationship describes the increase in lubricant viscosity with applied pressure. In high-pressure contacts such as gears and rolling element bearings, viscosity may increase by several orders of magnitude. Increased pressure reduces intermolecular spacing, limiting molecular mobility and increasing internal friction. This pressure-induced viscosity rise is fundamental to EHL lubrication, as it enables the formation of a load-carrying lubricant film. For most organic liquids, viscosity approximately doubles for every 0.05 GPa increase in pressure. Early work by Barus [14] reported a linear increase in viscosity with pressure:

$$\eta = \eta_0(1 + \alpha p) \quad (4)$$

where η_0 is the viscosity at ambient pressure and α is the pressure-viscosity coefficient. Later experiments by Hersey and Bridgman [15,16] demonstrated that viscosity increases more rapidly than linearly at higher pressures, with Bridgman observing an approximately exponential relationship between viscosity and pressure up to 1.2 GPa. This led to the widely used exponential form, often erroneously referred to as the Barus equation:

$$\eta = \eta_0 e^{\alpha p} \quad (5)$$

Another important model was proposed by Roelands [17,18], who introduced an empirical pressure-viscosity relationship incorporating a dimensionless pressure-viscosity index Z_1 . The Roelands model provides improved accuracy over the exponential form at moderate pressures and is commonly used in EHL analyses, particularly for inlet zone film thickness calculations. A relationship between the pressure-viscosity coefficient and the Roelands index was later proposed by Blok [19], enabling conversion between model parameters.

$$\eta = \eta_0 \exp \left[(\ln \eta_0 + 9.67) \left(\left(1 + \frac{p}{p_0} \right)^Z - 1 \right) \right] \quad (6)$$

$$Z_1 = \frac{\alpha}{(1/c_p)(\ln \eta_0 - \ln \eta_\infty)} \quad (7)$$

Despite their usefulness, both the exponential and Roelands models have limited validity at high pressures. Roelands suggested an upper applicability limit of approximately 0.5 GPa, beyond which these models tend to overestimate viscosity. As a result, they are generally unsuitable for accurately predicting viscosity in the high-pressure central regions of EHL contacts, where friction is governed. To address this,

modified multi-slope and higher-parameter empirical models have been proposed, though they often complicate the inclusion of temperature effects.

An alternative class of models is based on free volume theory, originally introduced by Doolittle [20] and later given physical interpretation by Cohen and Turnbull [21]. These models relate viscosity to the available free volume in the fluid and can describe the sharp viscosity increase near the glass transition. Extensions such as the Yasutomi–WLF model allow pressure effects to be incorporated without explicitly using an equation of state and have been further refined to improve low-pressure accuracy [22].

2.2.4 Equation of state

Although liquids are often treated as incompressible, this assumption is not valid in elastohydrodynamic lubrication (EHL) due to the very high pressures involved. Lubricants undergo significant, non-linear compression at pressures approaching 1 GPa, and neglecting compressibility would ignore the pressure-induced viscosity increase that enables load support in EHL contacts. Compressibility has a minor effect on minimum film thickness but a noticeable effect on the pressure-viscosity coefficient (PVC), commonly denoted as α , the central film thickness, which is approximately reduced in proportion to the relative volume compression [23,24].

To account for compressibility in EHL analyses, an equation of state (EOS) is required to relate lubricant volume or density to pressure and temperature. The most widely used EOS for high-pressure applications is the isothermal Tait equation [13], which expresses the volume relative to ambient pressure as:

$$\frac{V}{V_0} = 1 - \frac{1}{1 + K'_0} \ln \left[1 + \frac{p}{K_0} (1 + K'_0) \right] \quad (8)$$

where K_0 is the bulk modulus at ambient pressure and K'_0 is its pressure derivative. The corresponding pressure dependence of the bulk modulus is given by:

$$K = \left\{ 1 - \frac{1}{1 + K'_0} \ln \left[1 + \frac{p}{K_0} (1 + K'_0) \right] \right\} [K_0 + p(1 + K'_0)] \quad (9)$$

Temperature effects are incorporated through the temperature dependence of the ambient-pressure bulk modulus:

$$K_0 = K_{00} \exp(-\beta_K T) \quad (10)$$

and the thermal expansion of the lubricant volume:

$$\frac{V_0}{V_R} = 1 + a_v(T - T_R) \quad (11)$$

Together, these relations provide a complete EOS describing the compressibility of the lubricant as a function of pressure and temperature for EHL calculations.

2.2.5 Pressure-viscosity coefficient definitions

The pressure-viscosity coefficient (PVC) is commonly denoted as α , characterises the sensitivity of lubricant viscosity to pressure. For mineral and synthetic oils, α typically ranges between 15–25 GPa⁻¹ [13] resulting in substantial increases in viscosity under the high pressures encountered in EHL contacts. Several approaches are used to determine the PVC of lubricants:

- (a) Extraction from EHL film thickness measurements using empirical film thickness equations [25,26],
- (b) Direct high-pressure viscometry measurements [27],
- (c) Estimation from fluid physical properties [13],
- (d) Calculation from the adiabatic bulk modulus derived from sound velocity measurements [28].

Among these methods, the film thickness approach is most frequently reported in the literature, although it may introduce significant uncertainty [29]. In this method, α is inferred from measured central film thickness using analytical EHL correlations. For elliptical point contacts, the Hamrock–Dowson central film thickness equation is given by:

$$h_c = 2.69 R_x U^{0.67} G^{0.53} W^{-0.067} (1 - 0.61e^{-0.73k}) \quad (12)$$

From this relation, an explicit expression for the optically derived pressure-viscosity coefficient α_{opt} can be obtained as:

$$\alpha_{\text{opt}} = \frac{1}{E'} \left[\frac{h_c}{2.69 R_x (1 - 0.61e^{-0.73k})} U^{-0.67} W^{0.067} \right]^{\frac{1}{0.53}} \quad (13)$$

Leeuwen compared several EHL central film thickness formulas for circular contacts and recommended the Chittenden et al. approximation for PVC estimation from interferometric measurements [26]. However, such approaches may become unreliable when operating conditions or lubricant properties fall outside the empirical validity range of the equations. Since EHL film formation is strongly influenced by inlet conditions, factors such as shear thinning, thermal effects, and inlet pressure—none of which are explicitly included in classical film thickness equations can significantly affect optically derived PVC values [30].

Direct measurement of viscosity under pressure provides a more reliable characterisation of the pressure-viscosity response. Comparative studies by Hannon et al. [31] demonstrated that high-pressure viscometry yields more consistent PVC values, whereas optically inferred coefficients exhibit greater variability and require extensive datasets to conform to classical scaling relationships.

A falling-body viscometer can be used to measure viscosity and fall time at elevated pressures [32]. From measured viscosity-pressure data, different definitions of the pressure-viscosity coefficient can be obtained. The conventional pressure-viscosity coefficient, α_0 , is defined as the slope of the logarithmic viscosity and pressure curve at atmospheric pressure:

$$\alpha_0 = \left(\frac{d \ln \mu}{dp} \right)_{p=0} \quad (14)$$

The reciprocal asymptotic pressure-viscosity coefficient, α^* , is evaluated through piecewise integration of the pressure-viscosity curve following Bair's method [27], where the local pressure-viscosity coefficient between adjacent data points is approximated by finite differences:

$$\alpha^* = \left[\frac{\mu_0}{\alpha_N \mu_N} + \sum_{i=1}^{N-1} \frac{\mu_0 \mu_i - \mu_{i-1}}{\alpha_i \mu_i \mu_{i-1}} \right]^{-1} \quad (15)$$

$$\alpha_i = \frac{\ln \left(\frac{\mu_i}{\mu_{i-1}} \right)}{p_i - p_{i-1}} \quad (16)$$

Bair and co-workers [33] further introduced the universal pressure-viscosity coefficient, α_{film} , defined as:

$$\alpha_{\text{film}} = \frac{1 - e^{-k}}{p_{iv} \left(\frac{k}{\alpha^*} \right)} \quad (17)$$

where p_{iv} is the Blok integral,

$$p_{iv}(p) = \int_0^p \frac{\mu(0)}{\mu(p')} dp' \quad (18)$$

The pressure-viscosity coefficients α_0 , α^* , and α_{film} describe the piezoviscous response of a lubricant at different levels of approximation. The conventional coefficient α_0 is a local parameter that represents only the pressure-viscosity relationship near

atmospheric pressure and may not reflect the full pressure range relevant to EHL film formation. Bair and co-workers concluded that the coefficient should capture the overall pressure dependence of viscosity rather than just the initial slope at $p = 0$. Accordingly, the reciprocal asymptotic coefficient α^* is determined by piecewise integration of the measured viscosity–pressure curve, where each pressure interval contributes to the total isoviscous pressure [34]. Thus, α^* provides a weighted representation of the lubricant’s overall piezoviscous behaviour rather than a purely local derivative.

α_{film} is a scaled reciprocal of the Blok integral evaluated over the pressure range. The evaluation of α_{film} requires convergence of the Blok integral and is therefore applicable only to lubricants with a sufficiently strong piezoviscous response [35]. For fluids with negligible pressure–viscosity relation such as certain water-based lubricants, the integral does not converge, and α_{film} cannot be determined. Consequently, the α_{film} definition is most appropriate for lubricants exhibiting pronounced piezoviscous behaviour, such as mineral and synthetic oils.

2.3 Isothermal EHL film thickness equations

Analytical solutions of the full EHL problem require numerical methods; however, several empirical and semi-empirical approximation equations have been developed based on regression of numerical solutions. These equations provide practical tools for estimating central and minimum film thickness in engineering applications. Some of the equations for circular and elliptical contacts are listed below:

Hamrock & Dowson [36,37]

Central film thickness:

$$\frac{h_c}{R_x} = 2.69 U^{0.67} G^{0.53} W^{-0.067} \left(1 - 0.61 e^{-0.75 \left(\frac{R_y}{R_x} \right)^{0.64}} \right) \quad (19)$$

Minimum film thickness:

$$\frac{h_m}{R_x} = 3.63 U^{0.68} G^{0.49} W^{-0.073} \left(1 - e^{-0.70 \left(\frac{R_y}{R_x} \right)^{0.64}} \right) \quad (20)$$

Evans & Snidle [38]

Central film thickness:

$$\frac{h_c}{R_x (2U)^{0.5}} = 1.7 M^{-0.026} L^{0.40} \quad (21)$$

Minimum film thickness:

$$\frac{h_m}{R_x(2U)^{0.5}} = 1.9 M^{-0.17} L^{0.34} \quad (22)$$

Chittenden et al. [39]

Central film thickness:

$$\frac{h_c}{R_x} = 4.31 U^{0.68} G^{0.49} W^{-0.073} \left(1 - e^{-1.23 \left(\frac{R_y}{R_x} \right)^{\frac{2}{3}}} \right) \quad (23)$$

Minimum film thickness:

$$\frac{h_m}{R_x} = 3.68 U^{0.68} G^{0.49} W^{-0.073} \left(1 - e^{-0.67 \left(\frac{R_y}{R_x} \right)^{\frac{2}{3}}} \right) \quad (24)$$

Nijenbanning et al. [40]

Central film thickness:

$$\frac{h_c}{R_x(2U)^{0.5}} = \left[\left(H_{RI}^{\frac{3}{2}} + (H_{EI}^{-4} + H_{00}^{-4})^{-\frac{3}{8}} \right)^{\frac{2s}{3}} + (H_{RP}^{-8} + H_{EP}^{-8})^{-\frac{s}{8}} \right]^{\frac{1}{5}} \quad (25)$$

with:

$$D = \frac{R_x}{R_y}$$

$$s = 1.5 \left(1 + e^{-1.2 \left(\frac{H_{EI}}{H_{RI}} \right)} \right)$$

$$H_{00} = 1.8D^{-1}$$

$$H_{RI} = 145(1 + 0.796D^{14/15})^{-15/7} D^{-1} M^{-2}$$

$$H_{EI} = 3.18(1 + 0.006 \ln(D) + 0.63D^{4/7})^{-14/15} D^{-1/15} M^{-2/15}$$

$$H_{RP} = 1.29(1 + 0.691D)^{-2/3} L^{2/3}$$

$$H_{EP} = 1.48(1 + 0.006 \ln(D) + 0.63D^{4/7})^{-7/20} D^{-1/24} M^{-1/12} L^{3/4}$$

2.4 EHL regimes

EHL lubrication regimes describe how elastic deformation of the contacting solids and pressure-dependent lubricant viscosity interact to form a load-carrying lubricant film. The relative magnitude of these effects determines the operating lubrication regime and, consequently, the resulting film thickness. In fluid film lubrication, four main regimes can be identified depending on whether elastic deformation and pressure-viscosity effects are significant or negligible [41,42]. These regimes provide a systematic framework for analysing film thickness behaviour across a wide range of operating conditions. Four principal regimes of fluid film lubrication are discussed below along with corresponding mapping in Figure 3.

Isoviscous–rigid regime

In the isoviscous–rigid regime, elastic deformation of the contacting surfaces is negligible compared to the film thickness, and the maximum contact pressure is too low to produce any significant increase in lubricant viscosity. The lubricant therefore behaves as an isoviscous fluid, and the solids may be treated as rigid.

Example: lightly loaded contacts, such as circular arc thrust bearing pads.

Viscous–rigid regime

In the viscous–rigid regime, the contact pressure is sufficiently high to cause a noticeable increase in lubricant viscosity within the conjunction, while elastic deformation of the solids remains insignificant. Under these conditions, pressure-viscosity effects must be accounted for, but the surfaces can still be assumed rigid.

Example: Moderately loaded rolling contacts.

Isoviscous–elastic regime

The isoviscous–elastic regime arises when elastic deformation of the contacting solids is significant relative to the film thickness, but the contact pressure remains too low to induce a substantial increase in lubricant viscosity. This situation is characteristic of soft EHL and may be encountered in applications involving low-modulus materials.

Example: artificial joints, and elastomeric elements.

Viscous–elastic regime

In the viscous–elastic regime, both elastic deformation of the solids and pressure-induced increases in lubricant viscosity are significant. This regime corresponds to fully developed EHL lubrication and is typical of heavily loaded rolling and sliding contacts. The combined effects of elastic deformation and piezoviscous stiffening enable the formation of a continuous load-carrying lubricant film under very high contact pressures.

Example: ball and roller bearings, gears, and cams.

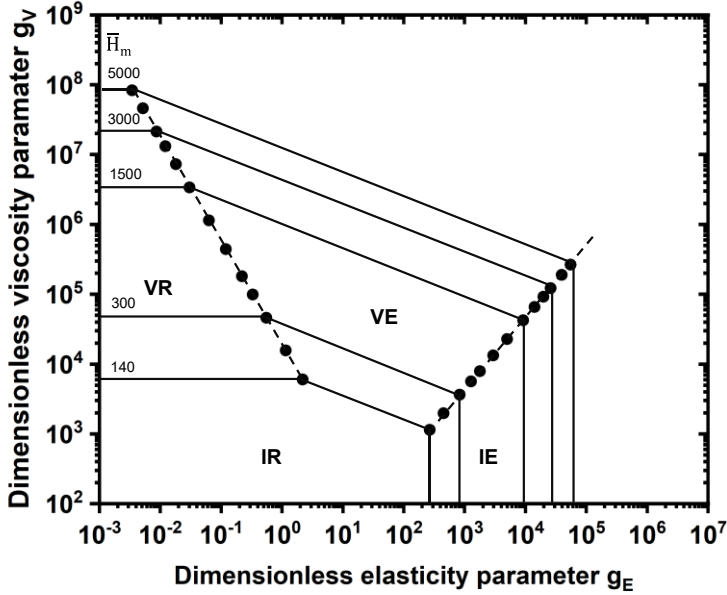


Figure 3: Maps of EHL lubrication regimes ($k=1$) [42]

The EHL regimes mapping is developed based on several dimensionless parameters. For elliptical contacts, the ellipticity parameter should also be considered to describe the contact geometry. The reduced set of dimensionless parameters governing EHL film thickness is:

$$(\hat{H}, g_v, g_E, k)$$

where \hat{H} is the dimensionless film thickness, g_v is the dimensionless viscosity parameter, g_E is the dimensionless elasticity parameter, and k is the ellipticity parameter. The classification of EHL regimes and the associated dimensionless parameters provide a powerful theoretical basis for understanding fluid film lubrication across a wide range of operating conditions. By reducing the complex elastohydrodynamic problem to a small number of physically meaningful dimensionless groups, it becomes possible to compare different lubrication regimes, predict film thickness trends, and identify transitions between rigid, elastic, isoviscous, and piezoviscous behaviour in practical engineering contacts.

2.5 Friction in rolling/sliding contact

Friction in rolling/sliding EHL contacts differs fundamentally from friction in purely hydrodynamic or boundary-lubricated systems. While film thickness is

determined by inlet conditions, friction is governed almost entirely by lubricant behaviour within the highly pressurised Hertzian zone [43].

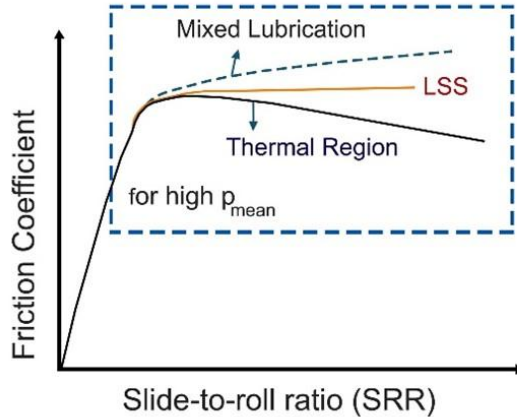


Figure 4: A schematic representation of the traction curve. LSS represents the limiting shear stress [44].

The coefficient of friction (CoF) in EHL contacts is defined as the ratio of the tangential (traction) force to the normal load and can be expressed in terms of the lubricant shear stress and contact pressure. Under pure rolling conditions, friction is minimal due to the absence of shear within the lubricant film. However, when sliding is introduced, shear stresses develop, leading to increased friction. A key parameter used to describe rolling/sliding conditions is the slide-to-roll ratio (SRR), which quantifies the relative sliding velocity between the surfaces. Experimental traction measurements show that EHL friction evolves through distinct regimes as SRR increases, as represented in Figure 4 and those are:

- Linear (Newtonian) regime: friction increases linearly with SRR at very low sliding.
- Non-linear regime: shear thinning and thermal effects begin to influence friction.
- Plateau regime: Friction reaches a maximum governed by the limiting shear stress.
- Thermoviscous regime: friction decreases at high SRR due to shear heating and viscosity reduction.

At high SRR values, significant frictional heat is generated within the contact. This local temperature rise reduces lubricant viscosity, leading to thermal softening and reduced traction. Consequently, friction in EHL contacts is strongly coupled to both lubricant rheology and thermal effects. Understanding friction in rolling/sliding EHL

contacts is essential for predicting efficiency, wear risk, and surface durability in heavily loaded machine elements such as gears and bearings.

2.6 Superlubricity in rolling/sliding contacts

Superlubricity is defined as a lubrication state in which the COF is extremely low, typically on the order of 10^{-2} or lower. Hirano and Shinjo introduced the term for atomic-scale “structural superlubricity” where atomically flat, incommensurate surfaces exhibit vanishing friction [45]. Although initially proposed for idealised solid–solid interfaces, superlubricity has been experimentally realised in practical systems, particularly under liquid lubrication conditions. In rolling/sliding contacts, superlubricity emerges from the combined action of fluid film formation and interfacial physicochemical effects that suppress shear resistance beyond the limits of conventional EHL lubrication [46].

From a rolling/sliding perspective, friction behaviour is commonly interpreted using the Stribeck framework, where friction is related to the Sommerfeld number $S = \eta u / p$. Experimental studies show that liquid superlubricity does not occur in pure boundary lubrication, but rather near the transition between mixed lubrication (ML) and EHL regimes [47]. In this region, a thin lubricant film partially or fully separates the surfaces, while friction is further reduced by interfacial mechanisms acting at the molecular scale.

Hydrodynamic and elastohydrodynamic effects play a necessary enabling role in rolling/sliding superlubricity. The formation of a converging lubricant wedge generates pressure that supports the applied load and reduces direct asperity contact. Superlubricity is strongly dependent on rolling or sliding speed and typically disappears at very low velocities, indicating that fluid film formation is essential. Moreover, friction in EHL contacts is mainly governed by viscous shear within the contact zone where pressure is highest. Fluids with a low pressure–viscosity response experience only a moderate increase in viscosity under pressure, resulting in lower viscous shear than conventional mineral oils having a high pressure–viscosity coefficient. This reduction in shear is likely a key factor behind the observed ultra-low friction [48]. However, additional mechanisms may also contribute, particularly in the presence of water content.

Besides low pressure–viscosity coefficient, reduction in shear resistance can also be enabled by hydration lubrication [49–51], particularly in water-based and aqueous lubrication systems. Strongly hydrated ions or charged surface groups form stable hydration layers that can withstand high normal pressures without being squeezed out, while simultaneously maintaining liquid-like shear behaviours. These hydration layers generate short-range repulsive forces that separate asperities and allow sliding with minimal energy dissipation, effectively resolving the trade-off between load-carrying capacity and low friction [52].

Rolling/sliding superlubricity is often preceded by a running-in process, during which surface roughness, chemistry, and interfacial structure evolve [53]. Running-in may smooth asperities, promote tribochemical reactions [54,55], and increase surface charge density [56], all of which enhance hydration lubrication and stabilise the superlubric state. Tribo-formed oxide or silica-rich surface layers, commonly observed in ceramic contacts, further reduce shear resistance and support sustained superlubricity under rolling-sliding conditions.

In summary, superlubricity in rolling/sliding contacts arises from a synergistic interaction between hydrodynamic or elasto-hydrodynamic film formation and interfacial shear-suppression mechanisms, particularly hydration lubrication. Rather than representing a distinct lubrication regime, rolling-sliding superlubricity can be viewed as an extension of mixed and EHL lubrication, where interfacial physics enables friction levels far below those predicted by classical lubrication theory.

2.7 Failure modes

Electric vehicle transmissions operate under conditions that differ significantly from those of conventional internal combustion engine drivetrains. These conditions are characterised by high rotational speeds, frequent torque reversals, high torque density, and extended service intervals [7]. Such operating characteristics strongly influence the dominant wear and failure mechanisms observed in gears and bearings, necessitating further design considerations to tackle unexpected failures. The major wear and failure modes affecting gears and bearings in EV transmissions are summarised in Table 1.

In EV gearboxes, gears and rolling bearings are subjected to high contact stress cycles arising from high-speed operation combined with low-to-moderate torque levels. In parallel, there is an increasing trend toward the use of low-viscosity lubricants to improve drivetrain efficiency, which can result in reduced EHL film thickness. Under these conditions, surface and subsurface fatigue mechanisms such as micropitting and macropitting may get intensified, creating favourable conditions for damage initiation and subsequent propagation.

Bearings in EV transmissions are particularly susceptible to additional challenges associated with electrification [57]. Inverter driven electric motors generate high-frequency voltage components and parasitic shaft currents [58,59], which may discharge through bearing contacts when the dielectric strength of the lubricant film is exceeded. These electrical discharge events cause localised surface melting followed by rapid quenching, leading to the formation of white etching areas and white layers. Such microstructural alterations act as stress concentrators, significantly reducing fatigue life and contributing to fluting or frosting phenomena, ultimately resulting in premature bearing failure accompanied by increased noise and vibration.

Table 1: Potential failure modes and consequences of gears and bearings in EV transmission.

Failure Mode	Primary Cause	Typical Consequences
Bending fatigue	Cyclic bending stress at the gear tooth root	Tooth fracture in gears
Micropitting / Macropitting	Surface and subsurface fatigue due to cyclic contact stress	Surface degradation, increased NVH in gears and bearings
Scuffing / Smearing	Lubricant film breakdown under high load or speed	Rapid surface damage on gear teeth and bearing raceways
Sliding / Adhesive wear (sliding wear)	Insufficient lubricant film thickness and continuous sliding between contacts	Material removal due to polishing effect, reduced service life of gears and bearings
Abrasive wear	Presence of contaminants or wear debris in the lubricant	Progressive profile wear in gears and bearing raceways
Plastic deformation	Contact stress exceeding material yield strength	Tooth profile distortion in gears, bearing raceway damage, increased NVH
Rolling contact fatigue (spalling)	Repeated Hertzian contact stress cycles	Surface spalling, increased friction, reduced bearing life
Corrosion / Chemical wear	Moisture ingress or lubricant oxidation and additive depletion	Surface pitting, reduction in fatigue life
Electric discharge-induced fluting (EDM)	Repeated electrical discharges through bearing contacts due to shaft currents	Raceway frosting and fluting, increased noise, premature bearing failure

Water-based lubricants (WBLs) offer potential environmental and frictional advantages; however, they also introduce significant challenges for EV gearbox applications. The inherently low viscosity and low pressure-viscosity coefficient of water-based lubricant increases the likelihood of film breakdown, promoting adhesive

wear and scuffing. In addition, gearbox components operating under WBLs may experience tribocorrosion, hydrogen-induced cracking, and aeration or foaming, all of which can adversely affect durability and reliability. Therefore, the successful implementation of water-based lubricants in EV transmissions will depend strongly on the development of advanced additive chemistries and surface protection strategies. Furthermore, the higher electrical conductivity of WBLs compared to traditional oils, and their effects on bearing currents and related damage, are not yet fully understood. Comprehensive tribological testing and microstructural characterisation are therefore essential to fully understand and ensure the long-term reliability of gears and bearings operating under such lubrication conditions.

2.8 Gearbox efficiency and power loss

The transmission system plays a crucial role in electric vehicle (EV) drivetrains since, unlike internal combustion engine powertrains, a significant portion of the overall propulsion losses occurs in the transmission. Gearbox losses may contribute approximately 15–25% of the total power losses in an electric vehicle, depending on the operating and driving conditions [60]. The gearbox efficiency is determined by the power losses generated in its mechanical components and is commonly defined as the ratio between the output power and the input power, according to:

$$\eta_{\text{gearbox}} = \frac{P_{\text{input}} - P_{\text{loss}}}{P_{\text{input}}} \quad (26)$$

In practice, gearbox loss maps are mostly obtained from experimental measurements, while explicit analytical computation of losses is less frequently adopted. However, reliable analytical models are valuable as they allow the estimation of gearbox efficiency and overall powertrain performance without extensive testing, supporting early-stage design decisions such as battery sizing.

Gearbox power losses arise from gears, bearings, seals, and auxiliary components [61]. These losses are commonly divided into load-dependent and load-independent losses. Load-independent losses occur even when no torque is transmitted and include effects such as lubricant churning, splashing, and windage. In contrast, load-dependent losses occur during power transmission and mainly result from friction in gear meshing and bearing operation. The magnitude of load-dependent losses depends on factors such as the applied load, friction between contacting surfaces, and rotational speed. Load-independent losses are primarily influenced by rotational speed and lubricant properties, including density and viscosity. In addition, design and operating factors such as housing configuration [62,63], lubricant immersion depth [64], and lubricant aeration and surface tension [65,66] also affects no-load losses.

This distinction between load-dependent and load-independent losses is particularly important for EV applications, where high rotational speeds and relatively low average torque cause speed-dependent losses to represent a significant share of the total transmission losses. Therefore, lubricant physical properties are of great importance to reduce losses alongside transmission mechanical design factors.

CHAPTER 3

3 Background & Research Gap

Chapter 3 provides a comprehensive review of the state of the art in water-based lubrication, with particular emphasis on rolling/sliding contact applications. Based on the literature review, key research gaps are identified, and the research objectives are formulated accordingly.

3.1 State of the art

Water-based lubricants (WBLs) have attracted increasing attention across a wide range of engineering applications due to their sustainability, environmental compatibility, and potential to improve energy efficiency. Although they have historically been used in cutting and hydraulic applications [67–69], recent research has focused on their applicability in complex mechanical systems. Lubricant manufacturers have begun to explore WBLs even for demanding applications such as automotive and electric vehicle transmissions, where mineral and synthetic oils have traditionally been used and proven reliable over several decades [5,70,71]. Although the development of WBLs is still at a relatively early stage, they are widely regarded as promising candidates for next-generation green lubrication technologies.

The direct use of water as a lubricant remains impractical for applications involving high loads or extreme operating conditions. Water exhibits very low viscosity and negligible pressure-viscosity dependence, limiting its ability to form a protective lubricating film between contacting surfaces [2]. Consequently, pure water alone cannot provide sufficient load-carrying capacity and wear protection. To overcome these limitations, water is commonly combined with water-soluble base fluids or additives, such as polyalkylene glycols (PAGs), polyethylene glycol (PEG), glycerol, and ionic liquids, to enhance the tribological performance of WBLs [3]. Research on these formulations has primarily focused on friction reduction and the achievement of superlubricity. However, significant research efforts have also been directed towards film formation, high-pressure rheological behaviour, wear protection and associated additive chemistry, as well as drag losses and efficiency in relation to physical properties. A brief discussion of the existing literature is presented below.

Friction behaviour and superlubricity

Superlubricity, commonly defined as a friction coefficient below 0.01, was originally predicted and observed at nanoscale crystalline solid interfaces, but over the past two decades it has increasingly been realised in macroscale liquid-lubricated rolling/sliding contacts using polyhydric alcohols such as glycerol and glycols.

Early indications that liquid-assisted superlubricity might be feasible in engineering contacts came from DLC-based systems. Kano [72,73] reported “super low friction” in engine components employing DLC coatings and lubricants, and De Barros Bouchet [74,75] subsequently demonstrated superlubricity in ta-C/DLC contacts lubricated with glycerol at elevated temperature, reaching friction below 0.01. These results established glycerol as an effective green lubricant, particularly when paired with chemically inert, low-shear carbon coatings. A step toward understanding the mechanism in metallic contacts was made by Joly-Pottuz et al. [76], who observed anomalously low friction in highly polished steel–steel contacts lubricated by glycerol, in some cases entering the superlubric regime. They proposed an “H-bond network” mechanism in which glycerol’s multiple hydroxyl groups form extensive intermolecular hydrogen bonds and, under sliding, partially decompose to generate water-like species that create a nanometer-scale hydrated film capable of supporting load while shearing easily [76–78]. This shifted the conceptual framework from classical boundary lubrication toward hydration-assisted superlubricity in polar liquids. Water generated from tribo-degradation of glycerol can form a low-viscosity, water-like phase within the hydrogen-bond network, further facilitating shear and reducing friction. This pressure-dependent mechanism becomes particularly significant at glycerol concentrations exceeding 80 wt.% [79].

Glycerol aqueous solutions exhibit significantly lower friction than rapeseed oil in both boundary and EHL regimes, with optimal friction reduction at 10–20 wt. % water content [80]. Hydration lubrication in water-based systems was further studied by Li et al. [81], who achieved $\text{CoF} \approx 0.003$ in phosphoric acid solution, attributing ultra-low friction to a stable hydrated acid–water network. They extended this to polyhydroxy alcohol–acid mixtures (including glycerol), where strengthened hydrogen-bond networks and in situ water generation enabled superlubricity [82]. Chen et al. [83] showed that low friction in glycerol–water lubrication of steel depends strongly on relative humidity, confirming that adsorbed water and hydrogen-bonded hydration layers govern the superlubric state. Later on, Shi et al. [80] showed glycerol aqueous solution exhibit significantly lower friction than rapeseed oil in both boundary and EHL regime and reported optimal friction reduction at 10–20 wt.% water content.

Under rolling/sliding and high-pressure conditions, Long et al. [84] reported superlubricity in steel/ta-C contacts with glycerol, proposing a tribochemical polishing mechanism involving FeOOH layers and hydrogen-terminated low-shear interfaces, supported by a thin EHL film. Björling and Shi [46] demonstrated to achieve

superlubricity under EHL rolling/sliding contacts using DLC and glycerol, attributing the effect to glycerol's low pressure-viscosity coefficient and high temperature sensitivity, together with DLC's thermal insulation, described as thermally assisted liquid superlubricity.

More recent studies emphasise compositional optimisation and molecular design. Ma et al. [85] identified an optimal water content (~ 20 wt.%) in glycerol-water mixtures that minimises friction. In a related study, Ma et al. [86] showed that glycerol blended with 1,3-propanediol achieves $\text{CoF} < 0.01$, whereas its isomer 1,2-propanediol does not contribute to stronger hydrogen bonding and better surface adsorption in the 1,3-propanediol system, highlighting the role of molecular architecture. Additive strategies further improved performance: Hua et al. [87] demonstrated that small amounts of ionic liquid in glycerol stabilise hydration layers and enable superlubricity even under thin-film conditions, independent of ambient humidity. Extending mixture design, Ma et al. [88] reported $\text{CoF} \approx 0.0057$ with negligible wear using optimised ethylene glycol/glycerol blends, supported by simulations showing interfacial enrichment and formation of low shear tribochemical species. In ethylene glycol (EG)-water systems, a stable $[\text{H}_2\text{O}]_m \cdot [\text{EG}]_n$ adsorption layer has been found to promote low friction and enhanced surface wettability friction [89].

Finally, the rolling/sliding elastohydrodynamic lubrication (EHL) perspective has recently been clarified by several researchers, who demonstrated that glycerol, PAG, and PEG-based aqueous lubricants can achieve superlubricity in rolling/sliding contacts even without tribochemical reactions being strictly required, provided that sufficient film thickness is maintained and operating parameters are properly optimized [90–93].

Overall, the chronological development of research on glycerol, glycols, and their aqueous solutions converges on a consistent mechanistic picture: superlubricity in rolling/sliding contact arises from one or synergy of the following actions:

- (a) Strong hydrogen bonding and hydration-layer formation
- (b) Surface adsorption/passivation, often reinforced by tribochemical films (e.g., FeOOH or carbon-rich layers),
- (c) Optimised viscosity and low pressure-viscosity coefficient.

Together, these effects enable CoF values in the 0.001–0.01 range, even at high contact pressures and under realistic rolling/sliding EHL conditions.

Pressure-viscosity behaviour and film formation

While low friction is desirable, adequate EHL film formation is essential for load-carrying capacity and surface protection. The pressure-viscosity coefficient is a key parameter governing EHL film thickness. Fluids with layered molecular structures typically exhibit low PVC values ($<10 \text{ GPa}^{-1}$), whereas fluids with highly entangled molecular architectures show stronger pressure-viscosity responses and higher PVCs ($>20 \text{ GPa}^{-1}$) [94]. Conventional mineral and synthetic oils are strongly piezoviscous and can therefore generate substantial EHL films under high contact pressures. However, high-pressure rheological behaviour of WBLs is not widely studied. Therefore, understanding pressure-viscosity behaviour and EHL film formation is critical to ensure sufficient load support, reduce friction, and avoid premature failure.

Studies on water-soluble compounds such as PAGs and glycerol have revealed complex film formation behaviour. Zhang et al. [95] showed that PAG solutions with high water content exhibit poor film-forming capability due to reduced viscosity, whereas low water concentrations can enhance film thickness through hydrogen bonding between PAG and water molecules. A concentration dependent solution-gel transition was also observed, with highly concentrated PAG formulations exhibiting gel-like behaviour and producing thinner films, while dilute solutions formed thicker films than predicted [96]. A recent paper shows film formation in aqueous EHL lubrication is governed by the ability of PAG polymers to penetrate to contact zone, which is enhanced by a mix of short and long PAG molecules along with optimised solvent polarity [97].

Glycerol-based systems exhibit similarly low pressure-viscosity responses. Shi et al. [80] reported film-derived PVC values of approximately 4.9 GPa^{-1} for pure glycerol and 4 GPa^{-1} for a glycerol-water solution containing 30 wt.% water. Stable EHL behaviour was observed below 30 wt.% water, whereas higher water contents led to a transition in the lubrication regime and a significant reduction in film thickness. These trends were confirmed numerically by Habchi et al. [77] who predicted an order-of-magnitude reduction in film thickness at 40 wt.% water content. Comparable effects were reported for PEG-based systems, where classical film thickness-velocity scaling was maintained until a sudden local film collapse below approximately 100 nm occurred, attributed to changes in molecular orientation and reduced adsorbed layers [90].

Despite their low PVC, several studies have shown that water-containing PAG-based lubricants can achieve film thicknesses comparable to those of conventional oils. Investigations at the Gear Research Centre (FZG), Munich, demonstrated that water-containing PAG formulations produce only slightly lower film thicknesses than polyalphaolefins (PAO) of similar viscosity [86]. Hofmann et al. [93] reported nearly identical film thicknesses for PAG-based fluids and PAO-05, despite the PAG fluid exhibiting nearly half the PVC. This behaviour was attributed to low water content and higher density compensating for the weaker pressure-viscosity response. More recent

work also showed that water evaporation increases both friction and film thickness, while maintaining low friction levels even at reduced water concentration [98].

Power loss and thermal behaviour

Reducing frictional losses is particularly important in electric vehicle powertrains, where gearbox losses can account for approximately 15–25% of total system energy losses, depending on operating conditions [60]. Lower friction directly reduces load-dependent losses, improving transmission efficiency and enabling more effective utilisation of energy from the electric motor. In this context, WBLs have attracted growing interest due to their potential to reduce both friction and power losses.

Yilmaz et al. [99] investigated the power loss behaviour of bearings lubricated with water-containing PAG fluids, reporting reduced no-load losses but increased load-dependent losses at elevated rotational speeds. Complementary simulations by Morhard et al. [100] suggested that a mono-fluid circuit using a glycol-based aqueous lubricant could reduce overall gearbox energy demand by approximately 2.2%. Hofmann et al. [101] further examined the influence of water evaporation on gear power losses and showed that although total power losses increase as water evaporates, load-dependent loss torque remains lower than that of conventional lubricants.

Friction between gearbox components is also the primary source of heat generation, with tooth friction being the dominant contributor [102,103]. If frictional heat is not dissipated effectively, sump temperatures rise, degrading performance and accelerating failure. The lubricant, therefore, plays a critical role as a cooling medium. Glycol-based aqueous lubricants exhibit significantly higher thermal conductivity and specific heat capacity than conventional electrical transmission fluids [104,105]. Combined with their low-friction behaviour, these thermal properties suggest strong potential for improving both efficiency and thermal management in EV transmissions.

Wear behaviour and additive effects

Wear performance remains a critical challenge for the industrial adoption of WBLs. Glycerol has been shown to produce negligible wear when used with surface-engineered materials such as DLC or ta-C coatings [7,9–12]. However, glycerol dissociation can also generate organic acids and aldehydes, introducing the risk of corrosive wear on uncoated steel surfaces. Despite this, most studies on glycerol-based lubrication have focused primarily on friction, with limited analysis of wear mechanisms.

Pure glycerol exhibits wear volumes comparable to rapeseed oil [80], whereas its aqueous solutions tend to accelerate wear. Tamayo et al. [6] reported mild wear under aqueous glycerol lubrication, which helped remove micro-crack nucleation during micropitting tests, while the addition of glycols significantly reduced wear. Bosch et al. [106] observed increased wear with water-rich formulations, attributing this to corrosion

product formation. In many of these literatures, the presence of anti-wear additives was not explicitly considered, despite their known importance. A recent study has focused on fully formulated WBLs for bearing testing and reported wear is the reason behind the early failure [107].

Recent studies demonstrate that appropriate additives can significantly enhance wear and corrosion resistance. Amine-functional additives effectively reduce wear in WBLs [108], while ionic liquids act as multifunctional friction-modifying and anti-wear agents by forming protective, oxide-rich tribolayers under sliding [109,110]. Additive-containing WBLs have also shown improved corrosion resistance, with no visible corrosion observed on steel surfaces during static tests [107].

3.2 Identified research gaps

Despite the growing interest in water-based lubricants (WBLs) for sustainable mobility applications, research focusing on rolling/sliding contacts representative of machine components remains limited. Most existing studies address fundamental tribological mechanisms rather than application-oriented investigations relevant to real transmission components. Based on the literature survey, the following research gaps have been identified.

1. Application oriented evaluation of WBLs

A comprehensive, application-focused comparison of major formulated WBL technologies is largely absent from the literature. In particular, systematic studies evaluating the tribological performance of different WBL formulations against conventional reference gear oils under identical operating conditions are scarce. This limits the assessment of the true potential of WBLs for practical transmission applications.

2. Friction and superlubricity

Most superlubricity studies in water-based lubrication have been conducted under highly specific and idealised conditions, often involving coatings, highly polished surfaces, or narrow operating windows. While these studies provide valuable insight into underlying friction-reduction mechanisms, the transferability of the results to uncoated steel-steel contacts with engineering-level surface roughness and to realistic transmission conditions remains uncertain. Furthermore, long-term friction stability under varying loads, speeds, temperatures, and water contents has not been sufficiently investigated.

3. Pressure-viscosity behaviour and film formation

Although several studies report low pressure-viscosity coefficients (PVC) and corresponding EHL film thickness behaviour for water-soluble lubricants, inconsistencies persist in PVC measurement methodologies and reported values. Moreover, the

applicability of conventional analytical film thickness equations to WBLs has not been critically assessed and is often assumed without validation. The combined influence of water concentration and temperature on the pressure-viscosity response and film formation behaviour of WBLs also remains insufficiently understood.

4. Power loss and thermal behaviour

Research on drag losses and efficiency in water-based lubricated transmissions is still limited, with most studies focusing on isolated components or simplified test rigs. Although reductions in no-load losses and improvements in thermal management have been reported in a few studies, the combined effects of friction reduction, water evaporation, and evolving lubricant properties on load-dependent losses under realistic gearbox operating conditions are not yet fully characterised. In particular, the long-term impact of water content variation on efficiency, thermal balance, and operational stability requires further investigation.

5. Wear behaviour and additives

Compared to friction and film formation, wear behaviour in water-based lubrication systems remains relatively underexplored. Existing studies often lack a systematic analysis of wear mechanisms, particularly for steel–steel contacts operating under mixed or boundary lubrication regimes. While the role of additives in mitigating wear and corrosion is widely acknowledged, their effects on WBL formulations are not consistently investigated. Moreover, the presence of water introduces the risk of corrosion and chemically driven wear; however, apart from static corrosion tests, comprehensive studies addressing corrosion-related wear under dynamic tribological conditions are largely absent from the literature.

3.3 Research questions

This doctoral research aims to investigate the potential of water-based lubricants for rolling/sliding contact applications, with the study structured around the following research questions:

1. Under what operating conditions do fully formulated water-based lubricants approach superlubricity in engineering surfaces, and how does their friction behaviour vary across lubrication regimes?
2. How do fully formulated water-based lubricants perform during long-duration tribotest under mixed and boundary lubrication, and what governs their wear behaviour: bulk lubricant properties, additive chemistry, or both?
3. Can water-based lubricants with high water content generate sufficient elastohydrodynamic film thickness, and are classical EHL film thickness models applicable to these fluids?
4. What are the pressure-viscosity coefficients of water-based lubricants, and how do water content and temperature influence their pressure-viscosity response?
5. Can water-based lubricants improve gearbox efficiency through reduced friction losses, or do increased water density and associated drag losses offset these benefits?
6. Does the presence of water promote tribocorrosion or chemically driven wear, and can additive systems mitigate this degradation

4 Experimental Methodology

Chapter 4 presents details of the tested lubricants, including their physical properties, as well as the experimental setups and procedures. It also describes the post-characterisation techniques used for analysis.

4.1 Candidate lubricants

Five lubricants were evaluated in this thesis. A fully formulated polyalphaolefin (PAO)-based gear oil was used as a reference lubricant, and four water-based formulations were developed for EV transmission applications. The water-based lubricants represented three different fluid technologies: glycol-water, glycerol-water, and ionic liquid-water systems.

Table 2: Test lubricants and their physical properties

Candidates	Composition	Water content (%)	Viscosity 40 °C (mPa.s)	Density 15 °C (gm/cm ³)	Refractive index 23 °C
R1	Formulated PAO based Gear oil	--	24	828	1.455
A1	Glycol + Water+ Additives	50-60 %	28	1075-1090	1.395
B1	Glycol + Water+ Additives	40-60 %	30	1080	1.409
C2	Glycerol +Water+ Additives	5-15 %	76	1235	1.455
D3	Ionic Liquid + Water + Additives	50-70 %	30	1136	1.404

Two glycol-water formulations, denoted A1 and B1, contained glycol as the base fluid with a moderately high-water content (50-60 %). The glycerol-water

formulation, C2, contained a lower water fraction (5–15 %) and exhibited the highest viscosity among the tested water-based lubricants. The ionic liquid-water formulation, D3, comprised an ionic liquid mixed with water (50–70 %) along with functional additives. All candidate lubricants were fully formulated by their respective suppliers to meet the operating requirements of electric vehicle transmissions. The key physical properties of the tested lubricants are summarised in Table 2.

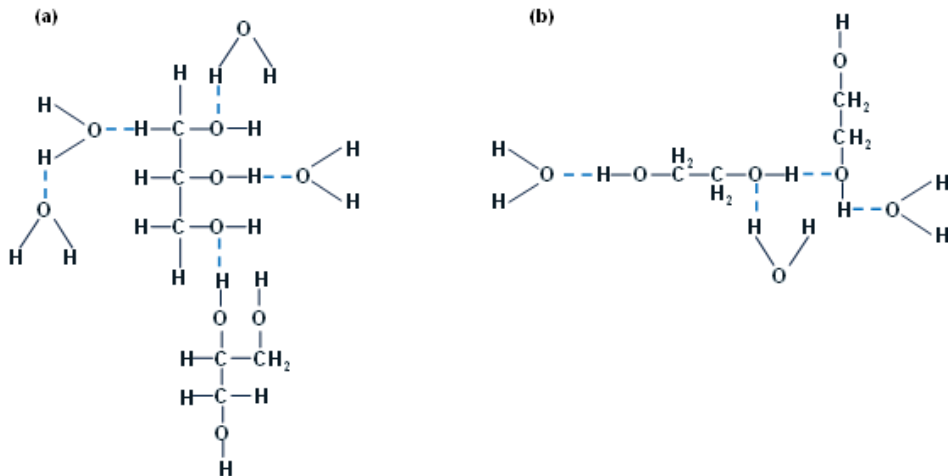


Figure 5: Schematic presentation of bonds present in (a) glycerol-water and (b) glycol-water mixture. Hydrogen bonds are highlighted.

Glycerol has three $-OH$ groups, which produce a great deal of intermolecular hydrogen bonds that result in the highest viscosity liquid out of all the technologies studied in this paper. When water is mixed with glycerol, it forms strong hydrogen bonds with water molecules and thus prevents water from evaporating at atmospheric conditions. Earlier studies found that glycerol and water form hydrogen-bonded clusters where an extensive glycerol-rich interface protects a low-density water-rich cluster [42].

Secondly, the glycol-water mixture consists of glycol, water, and additives. The simplest form of glycol, ethylene glycol, can be used here as an example. Ethylene glycol contains two polar $-OH$ groups, and both of them can form hydrogen bonds. This polarity results in attraction between ethylene glycol molecules, making them more difficult to separate. Therefore, due to the attractive forces between its molecules, ethylene glycol has a higher boiling point than hydrocarbons of similar mass. Ethylene glycol and water molecules can establish hydrogen bonds with each other, similar to their interactions at the individual molecular level. This property enables them to mix seamlessly in any proportion. The interaction of water with glycerol and glycol molecules is illustrated in Fig. 5.

The third candidate is a hybrid solution containing ionic liquid, water, sodium propionate, and additives. The water molecule itself has an ionic character as the positive charges of hydrogen adhere to oxygen by a covalent bond [43]. Meanwhile, sodium propionate molecules also contain positively charged sodium (Na^+) and negatively charged carboxylate ($\text{C}_2\text{H}_5\text{COO}^-$) ions. Therefore, the attraction can be defined as an ionic bond between the charged molecules.

4.2 Tribotesting: ball on disc tribometer

Friction, wear, and EHL film thickness measurements were conducted using two ball-on-disc tribometers: a WAM (Wedeven Associates Machine) and an MTM2 (Mini Traction Machine). The WAM was employed to investigate short-duration friction behaviour, such as traction and Stribeck curves, and EHL film thickness measurements under well-controlled rolling/sliding conditions, while the MTM2 was used for long-duration (18.5 hours) friction, wear, and tribofilm evolution studies. In both systems, the ball and disc were driven independently, enabling precise control of entrainment speed and the slide-to-roll ratio (SRR).

4.2.1 Stribeck and traction measurements (WAM)

For the Stribeck and traction curve measurements (Paper B), a WAM tribometer was employed. A polished steel ball with a diameter of 20.63 mm and a steel disc with a diameter of 101 mm were used. The corresponding root mean square surface roughness values were approximately 10 nm and 180 nm. All tests were conducted at a Hertzian contact pressure of 1.5 GPa and bulk lubricant temperatures of 40 °C, 60 °C, and 80 °C. Traction curves were obtained by varying the SRR from 0 to ± 0.65 at a fixed entrainment speed of 4 m/s, while Stribeck curves were generated by varying the entrainment speed between 8 m/s and 0.1 m/s at a constant SRR of 0.1. Reported friction coefficients represent mean values from repeated tests.

4.2.2 EHL film thickness measurements (WAM)

Film thickness measurements were conducted using an optical interferometry setup integrated into the WAM (Paper A). The lubricated contact was formed between a polished steel ball and a glass disc coated with a semi-reflective chromium layer. An additional transparent silica spacer layer was used to enable measurement of film thicknesses down to approximately 1 nm. Interference images generated under white-light illumination were captured with a microscope and a CCD camera to calculate the EHL film thickness as represented in Figure 6.

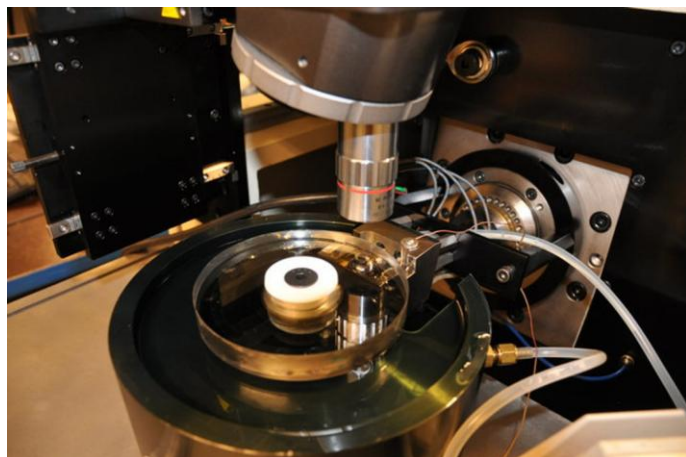


Figure 6: Ball on disc tribometer with optical attachments for film thickness measurements [111].

Film thickness tests were performed at a load of 25.7 N, corresponding to a maximum Hertzian pressure of approximately 0.5 GPa. Four water-based lubricants and one reference PAO-based oil were tested at 40 °C, 60 °C, and 80 °C. Measurements were initially conducted under pure rolling conditions, followed by tests with 10 % sliding to assess shear effects. Entrainment speed sweeps were carried out between 3 m/s and 0.1 m/s in both directions. Each test was repeated twice on a new track, and each data point represents the mean of four measurement sequences. Interferograms were processed using Achilles software, details of the process can be found here [112]. Prior to testing, the lubricant was circulated for 20 min to ensure thermal stability, and the lubricant was refreshed after each test to minimise water evaporation.

4.2.3 Wear and tribofilm studies (MTM2)

Extended friction and wear tests were conducted using a PCS MTM2 tribometer in a ball-on-disc configuration (Paper B). AISI 52100 steel balls (19.05 mm diameter) and steel discs (46 mm diameter) supplied by PCS Instruments were used. All experiments were performed under fully flooded lubrication conditions, with the bulk lubricant temperature controlled by an integrated heater. The friction pair was submerged in a lubricant chamber, and experiments were performed under fully flooded lubrication, with the bulk lubricant temperature controlled by an integrated heater.

Possible tribofilm formation during testing was monitored using spacer layer imaging (SLIM). At selected intervals, the ball was loaded against a spacer layer comprising a transparent SiO₂ coating with a semi-reflective chromium layer. Interference images generated under white light illumination were recorded to qualitatively assess tribofilm evolution. A schematic representation is shown in Figure 7.

The MTM2 tests aimed to investigate the time-dependent evolution of friction, wear, and the possible formation of tribofilms. All tests were conducted at an entrainment speed of 2 m/s and an SRR of 0.1, while the temperature was varied. Three water-based lubricants and one reference oil were tested at three temperatures each, with one repeat per condition, resulting in a total of 24 tests. Each test lasted up to 18.5 h, comprising a 0.5 h running-in period under pure rolling followed by 18 h of rolling/sliding operation. Inspections were performed at 2.5 h, 6.5 h, and 18.5 h to monitor friction behaviour and surface condition.

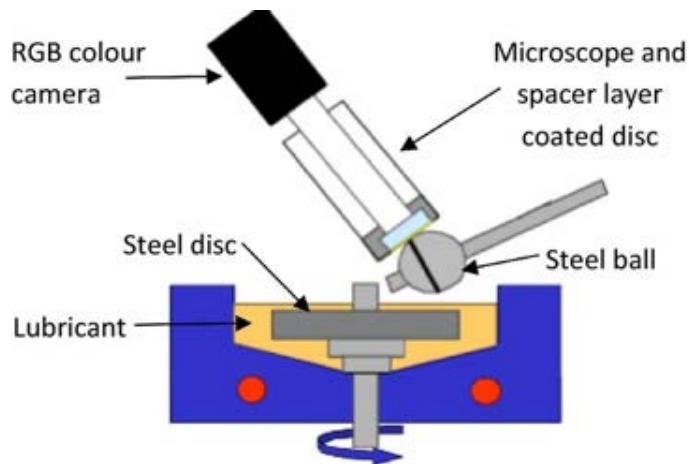


Figure 7: Schematic presentation of MTM–SLIM while capturing an image [113].

4.3 Pressure–viscosity coefficient determination

The pressure–viscosity coefficient, α , was determined using two independent approaches:

1. Extraction from EHL film thickness measurements (optical method)
2. Measurement using high-pressure falling body viscometer.

All measurements were evaluated at 40 °C to minimise evaporation effects in the water-based lubricants.

4.3.1 Film thickness derived pressure–viscosity coefficient

Central EHL film thickness measurement data were used to estimate the pressure–viscosity response following the approach described by van Leeuwen, i.e., by inverting a central film thickness relationship to obtain α . While the Hamrock–Dowson equation is commonly used for mineral/synthetic oils, it has been found unsuitable for

water-based fluids (See Section 5.1); therefore, the Nijenbanning central film thickness equation (equation 25) was used to determine the film thickness derived coefficient α_{opt} .

Optical interferometry provides film thickness from the optical path difference between reflected beams. For normal incidence, the measured optical thickness equals the product of the refractive index and the physical film thickness. Because refractive index varies with temperature and pressure, refractive index values were measured at ambient conditions (using an Abbe refractometer at ~ 23 °C and atmospheric pressure) and were corrected to the test conditions using the Lorenz–Lorentz relation, with density adjusted using the Tait equation. The corrected refractive index was then used in post-processing of interferograms to obtain the physical film thickness and, subsequently, α_{opt} via the inverted Nijenbanning approximation.

4.3.2 Viscometer derived pressure-viscosity coefficient

Pressure-viscosity behaviour was measured up to 500 MPa using a falling-body high-pressure viscometer based on Bair's method [27]. Measurements were taken at 10 pressure points using a solid sinker, and the fall time was recorded using an oscilloscope. A 20 min thermal stabilisation period was applied before each test. The viscometer was calibrated using trioctyl trimellitate (TOTM), and the estimated measurement uncertainties were approximately 5% (viscosity), 0.5 °C (temperature), and 0.6% (pressure) relative to published reference data [114]. In the falling-body method, viscosity is obtained from the measured fall time using the following expression:

$$\mu = Ct \frac{7.8 - \rho}{7} \quad (27)$$

where t is the sinker fall time (defined using a 1000 mV change in the LVDT signal), C is the calibration factor, and ρ is the fluid density. Density was measured at ambient conditions and extrapolated to the test condition using the Tait equation, employing recommended parameter values when lubricant-specific constants were unavailable. Pressure-viscosity coefficients measured using a high-pressure viscometer were reported using two common definitions (equations 14 and 15). Figure 8 shows a schematic representation of a high-pressure falling body viscometer.

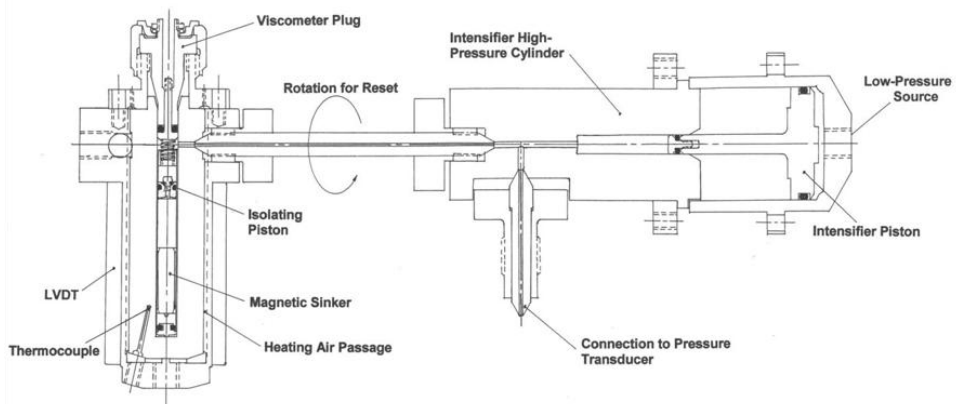


Figure 8: A schematic representation of a high-pressure falling body viscometer [32].

4.4 Drag loss and efficiency tests

Drag loss and transmission efficiency were evaluated using a dedicated test gearbox lubricated with three water-based lubricants and a fully formulated gear oil as a reference. The experimental setup, test configurations, and lubrication system are outlined in the following sections.

The unit under test (UUT) comprised a gearbox coupled to an electric drive system and was installed inside a climate-controlled chamber. An energy closed-loop configuration was employed, and the UUT arrangement was modified depending on whether drag torque or efficiency measurements were performed. Schematic illustrations of the two configurations are provided in Figures 9 and 10.

During drag torque testing, the UUT included the gearbox and an electric machine with both rotor and stator components, with the input dynamometer connected to the differential. For efficiency testing, the electric machine was removed and replaced by an extended stator shaft connected to an input dynamometer and a torque transducer. In this configuration, the gearbox transmitted power to the output shaft, where a second dynamometer measured the delivered power. The input dynamometer applied the required load, while the output dynamometer provided counter-torque to maintain the target operating speed. Transmission losses and efficiency were calculated from the difference between the input and output power.

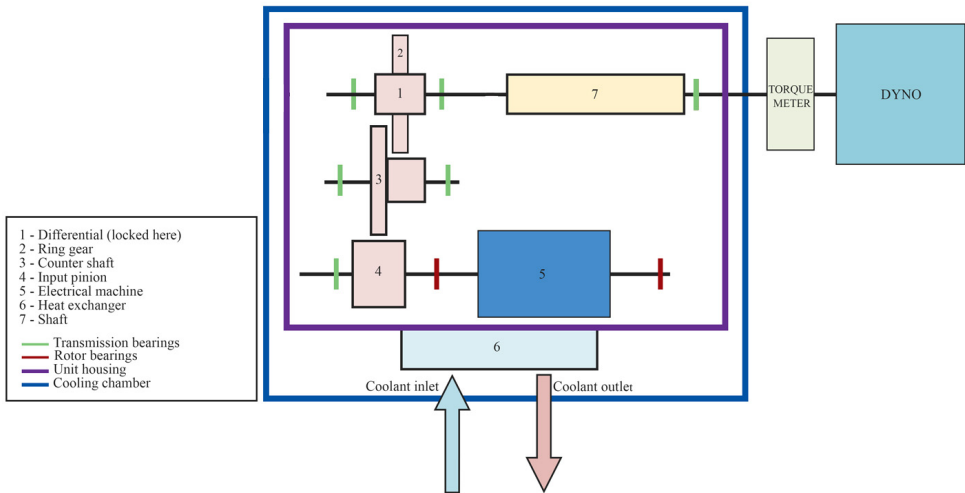


Figure 9: Schematic representation of the test rig assembly for the drag torque test.

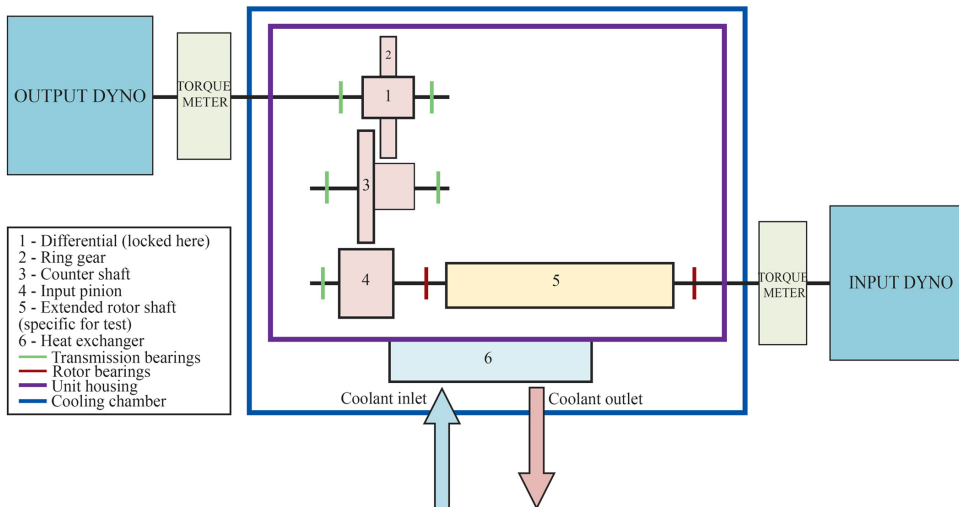


Figure 10: Schematic representation of the test rig assembly for the efficiency test.

The gearbox was lubricated with the selected candidate fluids. Lubricant was circulated from a reservoir through a filter and a heat exchanger, enabling precise temperature control during testing. Type-K thermocouples were positioned near the outer ring of the rotor bearings to monitor thermal conditions. After completing each test, the lubrication circuit and gearbox were drained and flushed using a suitable cleaning fluid. Before introducing the next lubricant, the system was flushed with a full charge of the new fluid to minimise cross-contamination. The filter element was replaced when switching between the reference oil and the WBLs. More details about the test setup and methodology are outlined in Paper C.

4.5 Tribocorrosion test

Tribocorrosion experiments were carried out using a reciprocating ball-on-disc configuration on a TE 79 tribometer integrated with an electrochemical cell as represented in Figure 11 (Paper D). Hardened carbon–chromium bearing steel specimens (SKF GS 81208) were polished with 400-grit SiC paper, ultrasonically cleaned in ethanol and acetone, and dried before testing. A 6 mm alumina inert ball was used as the counterbody.

A three-electrode electrochemical system was employed, where the steel specimen acted as the working electrode, Ag/AgCl as the reference electrode, and platinum wire as the counter electrode. All electrodes were connected to a Metrohm Autolab PGSTAT302N potentiostat.

Tests were conducted in three different glycerol solution with equal viscosity. Reciprocating sliding was performed with a 4 mm stroke length, 6 mm/s sliding speed, and 15 N normal load. The specimen was stabilised at open circuit potential (OCP) for 30 min, followed by 10 min at the selected potential, 20 min of sliding under constant potential, and 5 min post-sliding repassivation. Each condition was repeated three times. Linear polarisation measurements were also performed from -0.5 to $+0.5$ V vs OCP at 1 mV/s. Wear track topography and wear volume were measured using a Zygo NewView 9000 optical interferometer following ASTM G133-05. The chemical wear volume was calculated from the integrated anodic charge using Faraday's law.

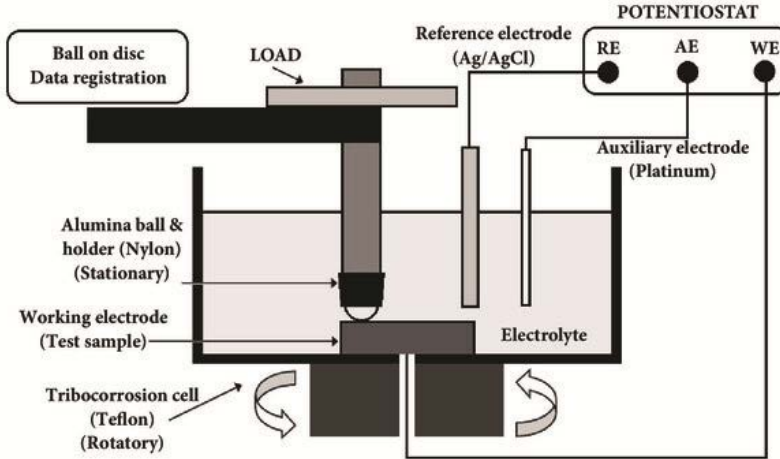


Figure 11: Schematic of the tribocorrosion test setup [115].

4.6 Surface characterisation

White Light Interferometry (WLI) was utilised to analyse Surface topography and wear features were analysed using a Zygo NewView 9000 optical interferometer. Areal measurements of the wear tracks were performed using a $10\times$ objective. Since a single scan did not cover the full wear scar width, multiple adjacent scans were acquired and combined through a stitching process, with each scan covering an area of $1.092\text{ mm} \times 0.468\text{ mm}$. Surface data were post-processed using MountainsMap 9 software, where overall form was removed by applying a second-order polynomial.

Detailed examination of surface morphology was carried out using a Zeiss Merlin field-emission scanning electron microscope (FEG-SEM). Imaging was performed in secondary electron mode using an accelerating voltage of 10 kV and a beam current of 10 nA.

Chemical and elemental analyses of the worn surfaces were conducted using X-ray photoelectron spectroscopy (XPS) with a Physical Electronics Quantera II Scanning XPS Microprobe. Prior to analysis, samples were cleaned with ethanol and ultrasonically treated in heptane for 5 min to minimise surface contamination. XPS measurements were performed both before and after sputter cleaning in order to distinguish surface-adsorbed species from the underlying material.

XPS Spectra were collected using a 100 μm X-ray beam, with pass energies of 224 eV for survey scans and 55 eV for high-resolution scans. Data acquisition was carried out with a time step of 50 ms and energy step sizes of 0.8 eV and 0.1 eV for survey and elemental scans, respectively. Sputter cleaning was performed at 500 eV over a 1 mm^2 area for 30 s on the wear track. Multiple scans were recorded to improve signal quality and reduce noise.

Hardness measurements were carried out using a NanoTest Vantage nanoindenter with a Berkovich diamond indenter. Indentations were performed up to a maximum load of 15 mN, with a 10 s dwell time, and hardness values were determined from 100 indentations inside and outside the wear track.

4.7 Fluid characterisation

Fourier transform infrared spectroscopy (FTIR) was employed to characterise the chemical functional groups of both fresh and tested lubricants. Measurements were performed using a Thermo Fisher Nicolet Summit spectrometer fitted with a diamond attenuated total reflectance (ATR) module. Each spectrum was collected from 10 co-added scans at a resolution of 4 cm^{-1} . Baseline correction was applied to all spectra using Spectragryph v1.2.16 software to remove background noise, artefacts, and environmental contributions, enabling consistent comparison between samples.

Dynamic viscosity was measured using an Anton Paar MCR 92 rheometer equipped with a concentric cylinder geometry. Tests were conducted over a logarithmically increasing shear rate range from 1 to 100 s^{-1} . Each measurement was repeated three times, and mean values are reported.

Thermogravimetric analysis (TGA) was carried out using a Mettler Toledo thermogravimetric analyser to quantify the water content of the water-based lubricants before and after testing. This technique monitors mass changes in a sample as a function of temperature under controlled heating conditions.

The refractive index of the lubricants was determined at ambient conditions using an Abbe refractometer. Fluid density was measured using an Anton Paar handheld density meter. These measurements were used to support optical film thickness analysis and property characterisation of the test fluids.

CHAPTER 5

5 Results

Chapter 5 presents the important results and outcomes of this project.

5.1 EHL film formation and pressure-viscosity relationship

The following discussion points summarise the findings regarding EHL film formation and rheological performance of water-based lubricants. Moreover, the applicability of the conventional EHL approximation is also discussed. More detailed discussion can be found in Paper A.

EHL film formation by WBLs

The EHL film formation of four water-based lubricants (WBLs) and a reference PAO-based gear oil was evaluated under pure rolling conditions. Figure 12 presents the central film thickness as a function of entrainment speed at 40 °C, together with the corresponding optical interferograms. Typical EHL characteristics were observed for all lubricants, with stable film shapes and no evidence of starvation. Minor film shape deformation was observed at the highest entrainment speeds, particularly for fluid C2.

Since the contact conditions and material properties were identical for all tests, variations in film thickness are primarily governed by fluid viscosity and pressure-viscosity response. The glycerol-water formulation (C2), possessing the highest viscosity, generated the greatest central film thickness, whereas the ionic liquid-water mixture (D3) produced the thinnest films, particularly at low entrainment speeds where its behaviour approached that of water. Despite having similar viscosities to A1 and B1, the reference PAO oil (R1) produced thicker films, which is attributed to its higher pressure-viscosity coefficient under high contact pressure. Overall, all formulated WBLs can generate adequate EHL films, regardless of their rheological differences, except for fluid D3.

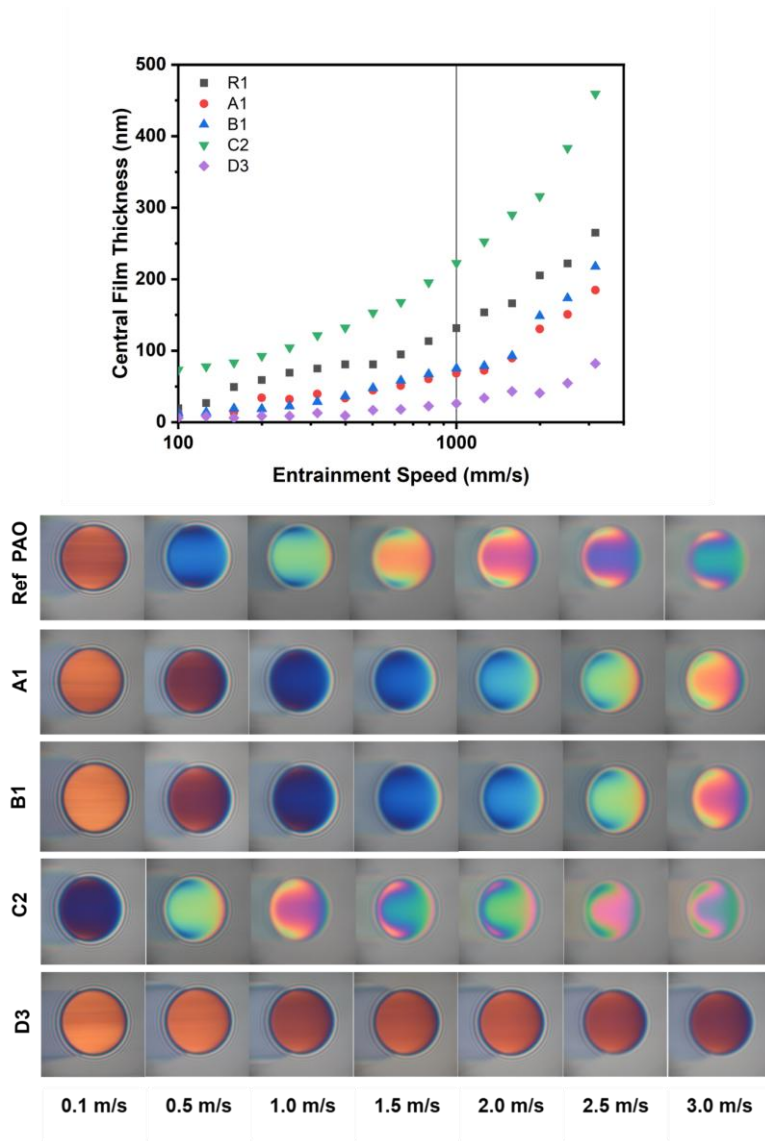


Figure 12: EHL film thickness measurements of WBLs and reference oil as a function of entrainment speed at 40°C and the corresponding interferograms.

Effect of operating parameters on film formation

The stability and thickness of the lubricant film are highly sensitive to several operational variables:

Entrainment speed significantly influences EHL film formation, with film thickness increasing consistently with speed. Higher speeds enhance lubricant entrainment into the contact inlet, promoting film build-up. This behaviour follows the classical EHL relationship, where film thickness increases approximately according to a power-law dependence on speed.

Temperature affects film formation primarily by modifying viscosity. While increasing temperature generally reduces film thickness due to reduced viscosity, water-based lubricants may exhibit atypical behaviour because water evaporation alters the fluid composition and increases effective viscosity. Some WBLs showed higher film thickness at elevated temperatures. This was attributed to water evaporation, which increased the concentration of the base lubricant and consequently increased viscosity.

Slide-to-Roll Ratios (SRRs) influence was evaluated by comparing pure rolling (SRR = 0%) and rolling/sliding conditions (SRR = 10%). The influence of SRR on film formation depends on lubricant composition. Most test lubricants showed negligible changes in film thickness under rolling/sliding conditions, whereas glycol-water lubricants exhibited increased film thickness at higher speeds, likely due to shear-induced concentration changes and viscosity modification within the contact inlet.

Pressure-viscosity coefficients

The pressure-viscosity coefficients (PVCs) were determined using both optical interferometry and high-pressure viscometry as discussed in section 4.3. The viscometry derived PVCs are summarised in Table 3. Based on viscosity measurement at the required pressure points, the conventional pressure-viscosity coefficient, α_0 and the reciprocal asymptotic pressure-viscosity coefficient, α^* , of the lubricants were calculated. α_0 can be calculated directly from the pressure-viscosity measurements, as represented in Fig. 13.

The lowest PVC value was observed for the ionic liquid-water solution (D3) (0.94 GPa^{-1}), whereas the PAO-based reference oil (R1) exhibited the highest value (15.25 GPa^{-1}). The glycol-water mixtures A1 and B1 showed similar PVCs of 2.20 and 2.93 GPa^{-1} , respectively, whereas the glycerol-water solution (C2) exhibited a higher PVC of 4.73 GPa^{-1} , consistent with its higher viscosity.

Table 3: High-pressure viscometer derived pressure-viscosity coefficients at 40°C

PVC (GPa ⁻¹)	Lubricants						
	R1	A1	B1	C2	D3	Glycerol	Glycol
$\alpha^*_{0.5 \text{ Gpa}}$	15.25	2.2	2.93	4.73	0.94	5.34	5.48
α_0	17.6	2.8	3.36	5.06	1.5	5.83	6.58

Table 4: Film thickness derived pressure-viscosity coefficients using film thickness approximations at 40°C

PVC (GPa ⁻¹)	Film thickness approximation	Lubricants				
		R1	A1	B1	C2	D3
α_{opt}	Nijenbanning et al.	12.83	1.01	1.41	4.22	0.20

Although higher viscosity often correlates with increased PVC within the same lubricant family, comparisons across fluids with different molecular structures are less straightforward. The WBLs investigated exhibited higher viscosities than the PAO oil at 40 °C but still showed lower PVCs. This behaviour is attributed to differences in molecular structure, as the branched hydrocarbon chains in PAO oils typically produce a stronger pressure-viscosity response.

PVCs were also estimated from optical film thickness measurements using established EHL film thickness equation (Table 4). For the PAO oil, the optically derived coefficient (α_{opt}) was approximately 15% lower than the viscometer-derived value (α^*), consistent with earlier reports and often attributed to shear-thinning effects during optical measurements. For the WBLs, the discrepancy between the two methods varied depending on the pressure-viscosity behaviour of the fluid. In the case of the glycerol-water solution (C2), the difference was within about 10%, whereas larger deviations were observed for glycol-water mixtures (A1 and B1), which have a poor pressure-viscosity response. This suggests that commonly used approximations may underestimate the PVC of fluids with relatively weak piezoviscous behaviour.

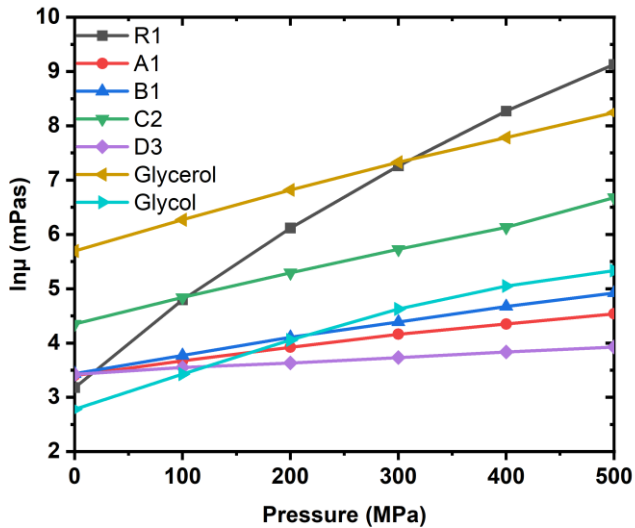


Figure 13: Pressure dependence of viscosity of all tested fluids. The logarithm of dynamic viscosity ($\ln\mu$) is plotted against pressure.

Effect of water content on pressure-viscosity coefficients

Temperature and water content both have a significant influence on the pressure-viscosity coefficient (α^*) of glycol- and glycerol-based lubricants. For all samples, α^* decreases with increasing temperature, indicating reduced viscosity sensitivity to pressure at higher temperatures. This effect is particularly pronounced for pure glycol and glycerol, where α^* decreases from 5.59 and 5.34 GPa^{-1} at 40 °C to 3.67 and 3.98 GPa^{-1} at 80 °C, respectively. The addition of water further modifies this behaviour. Glycol-water mixtures with high water content (50–60%) show a substantial reduction in α^* and a weaker temperature dependence compared to pure glycol. In contrast, the glycerol-water mixture with lower water content (5–15%) behaves similarly to pure glycerol. Overall, increasing water content lowers the pressure-viscosity coefficient and reduces the combined pressure and temperature sensitivity of viscosity.

Applicability of analytical film thickness equation for WBLs

The applicability of classical analytical film thickness equations for water-based lubricants was evaluated by comparing experimental results with existing EHL models. The lubrication regime analysis in Figure 14 showed that glycol-water lubricants operate near the boundary between isoviscous-elastic and viscous-elastic regimes, while ionic-liquid water solutions predominantly operate in the isoviscous-elastic regime where pressure-viscosity effects are minimal. In contrast, glycerol-water lubricants operate in a viscous-elastic (VE) regime, exhibiting behaviour somewhat similar to conventional piezoviscous oil under high contact pressure and entrainment speed.

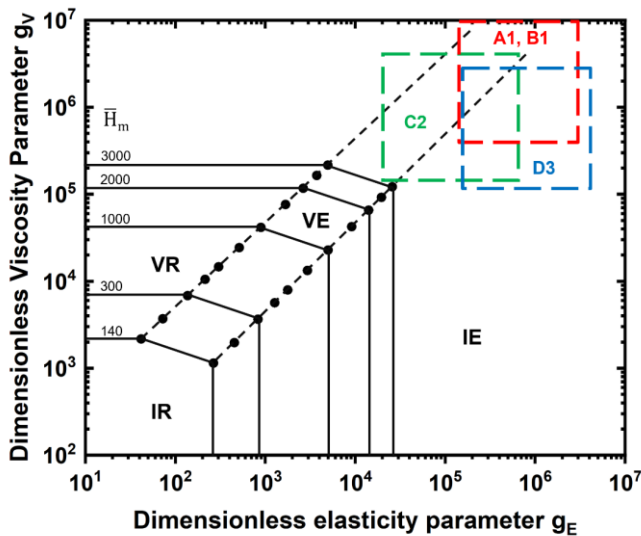


Figure 14: Map of lubrication regimes for circular point contact, along with operation zones for WBLs during the test

The soft EHL equation correlates well with experimental film thickness for WBLs with weak piezoviscous behaviour. However, it is insufficient for piezoviscous fluids such as glycerol-water (C2), where pressure-viscosity effects are significant. Therefore, film-thickness models incorporating pressure-viscosity coefficients are required for accurate prediction.

The applicability of the Hamrock-Dowson (HD) film thickness equation to water-based lubricants was evaluated by comparing experimental film thickness data with the classical speed-film thickness relationship. The HD theory predicts a power-law

dependence of film thickness on entrainment speed with an exponent of approximately 0.67 for conventional oils. Experimental results showed good agreement with this relationship for the reference PAO oil, confirming the validity of the HD equation for conventional lubricants. However, water-based lubricants exhibited different speed dependencies, with a glycerol–water lubricant (low water content) showing a lower speed exponent, whereas high-water-content fluids showed a stronger speed dependence, see Figure 15. These deviations suggest that lubricant composition, water content, and molecular structure influence the film-forming behaviour of WBLs, indicating that classical oil-based EHL models may not fully capture the film-thickness behaviour of water-based lubricants.

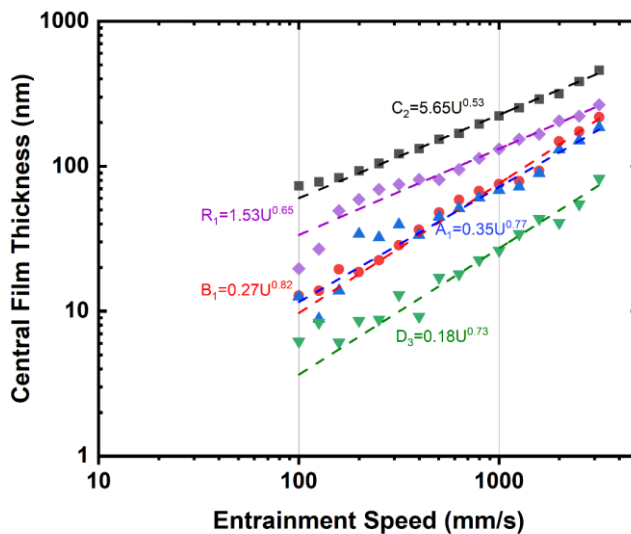


Figure 15: Central film thickness measurement of reference PAO-based oil (R1) and WBLs (A1, B1, C2 and D3) at 40°C and 0.5 GPa contact pressure

The validity of analytical film thickness models was assessed using the dimensionless load (M) and material (L) parameters, following the domains defined by Wheeler et al. The analysis showed that the operating conditions of the reference PAO oil fall within the applicability range of the Hamrock–Dowson model, whereas the operating zones of water-based lubricants lie outside this domain due to their significantly lower pressure–viscosity response. As a result, the Hamrock–Dowson equation may not accurately predict the film thickness behaviour of WBLs. Instead, the Nijenbanning film thickness equation appears more suitable, as it was developed over a wider range of Moes parameters and can accommodate cases with weak piezoviscous behaviour, including near-isoviscous conditions commonly observed in water-based lubricants.

5.2 Analysis of frictional behaviour

The frictional performance of the fully formulated WBLs A1, B1, and C2 demonstrates a substantial reduction in the coefficient of friction compared with the reference PAO gear oil (R1). Under high contact pressure and representative material and surface roughness conditions (AISI 52100 steel), the WBL formulations consistently outperform the conventional reference lubricant in terms of friction across the full lubrication regime. In this section, frictional behaviour is evaluated using Stribeck and traction curve analyses. In addition, friction stability during extended duration testing is assessed. Further details are provided in Paper B.

Stribeck regimes and the threshold of superlubricity

Figure 16 presents the Stribeck curves, showing the variation of the friction coefficient with rolling speed under representative contact conditions. Stribeck analysis shows a distinct transition from boundary lubrication at low entrainment speeds to full-film elastohydrodynamic lubrication as speeds increase.

At low rolling speeds, where boundary lubrication prevails, lubricant formulation plays a more dominant role due to increased surface interactions. The gear oil (R1) exhibited reduced friction at elevated temperatures compared to low-temperature cases, likely due to additive activation. This temperature-dependent friction behaviour was not significant for the WBLs, which maintained a relatively similar boundary friction coefficient of approximately 0.1.

As rolling speed increases and full-film EHL is established, friction decreases markedly for water-based lubricants (WBLs) due to reduced asperity contact. In this regime, friction is governed primarily by the rheological properties of lubricants rather than their chemical composition. Among the WBL formulations, the glycol-water lubricant (A1) exhibited the lowest friction (approximately 0.01 at 40 °C), approaching superlubricity at a rolling speed of 1 m/s and maintaining this behaviour at higher speeds. The achievement of superlubricity is markedly delayed for fluids B1 and C2 relative to A1.

B1 and C2 required higher speeds to reach comparable friction levels, reflecting differences in rheological properties and water content. At elevated temperatures (60 °C and 80 °C), reduced viscosity led to thinner films, and consequently, higher entrainment speeds were necessary to achieve superlubricity. For example, A1 required speeds above 3 m/s at 80 °C, compared with 1 m/s at 40 °C. Across all temperatures in the full-film regime, the reference PAO gear oil exhibited friction values at least four times higher than those of the WBLs.

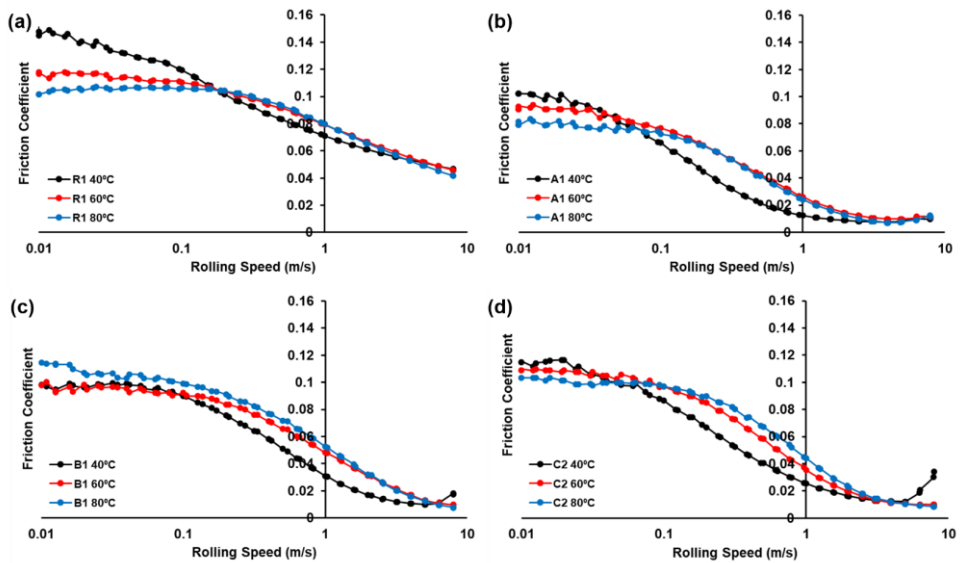


Figure 16: Stribeck curve as a function of entrainment speed of (a) reference oil R1, (b) glycol-water A1, (c) glycol-water B1, and (d) glycerol-water C2 solutions at $Ph=1.5$ GPa and $SRR=0.1$.

Traction behaviour

Traction behaviour was evaluated at an entrainment speed of 4 m/s over SRR values of ± 0.65 and temperatures of 40–80 °C (Figure 17). The reference oil exhibited a linear traction region at low SRR , followed by a non-linear increase to a maximum at approximately $SRR = 0.1$. At 40 °C, a transition to a thermal regime was observed at higher SRR , attributed to shear-induced viscosity reduction. At 60 °C and 80 °C, the traction curves reached an early plateau ($\approx \pm 0.15$ SRR), indicating the onset of limiting shear stress behaviour.

In contrast, the water-based lubricants (WBLs) demonstrated significantly lower friction under all conditions, with A1 achieving coefficients below 0.01 at 40 °C. Although similar traction regimes were identified, the increase in friction with SRR was more gradual, and a steady plateau was reached at approximately ± 0.20 SRR . At elevated temperatures, the WBLs showed indications of mixed lubrication, likely due to thinner film formation. Notably, WBLs exhibit a complete absence of the thermal region (shear-heating) typically observed in R1.

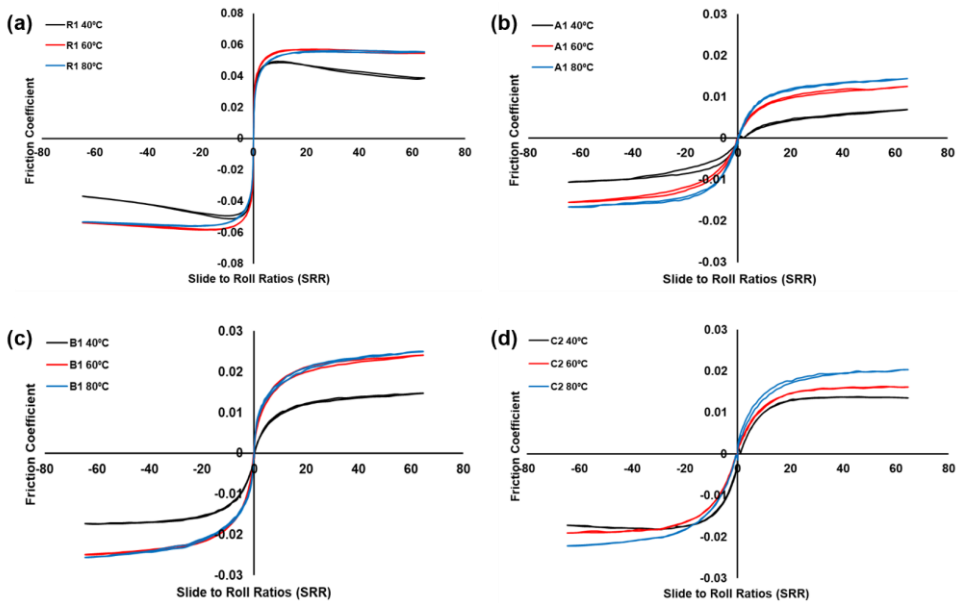


Figure 17: Traction curve as a function of the slide-to-roll ratios of (a) reference oil R1, (b) glycol-water A1, (c) glycol-water B1, and (d) glycerol-water C2 solutions at $P_h=1.5$ GPa and $U_c=4$ m/s

Long-duration friction stability

Figure 18 summarises the friction evolution during the 18.5-hour tests conducted using the MTM ball-on-disc configuration. All experiments began with a 0.5-hour running-in period under pure rolling conditions. Sliding was subsequently introduced, resulting in an immediate increase in friction. Each test was interrupted at three predefined intervals for surface evaluation, as discussed in the following section.

The reference oil (R1) exhibited the highest friction among all lubricants, although it maintained stable behaviour throughout the tests. A maximum coefficient of friction (CoF) of 0.09 was recorded at 60 °C. At 80 °C, friction decreased compared to 60 °C, likely due to enhanced additive activation at elevated temperature.

For the water-based lubricants (WBLs), higher temperatures (60 °C and 80 °C) led to an initial increase in friction, followed by a gradual reduction as the test progressed. The initial rise is attributed to reduced viscosity and increased asperity interactions, whereas the subsequent decrease suggests progressive surface modification. Overall, the glycerol-water formulation (C2) demonstrated comparatively stable frictional performance across the investigated temperature range compared to other WBLs.

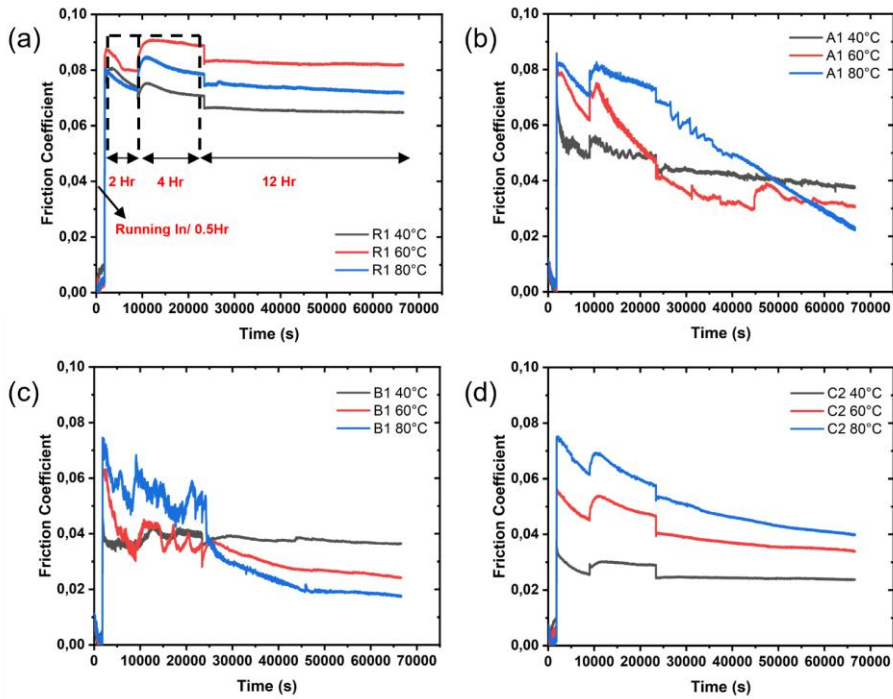


Figure 18: Average coefficient of friction over time during long duration test (a) reference oil R1, (b) glycol-water A1, (c) glycol-water B1, (d) glycerol-water C2 solutions at $Ph=1.25$ GPa, $U_e=2$ m/s and $SRR=0.1$

5.3 Wear evolution and characterisation

Surface modification, possible tribofilm formation, and wear evolution during the long-duration friction tests are discussed in this section. During the 18.5-hour tests, the experiments were paused at 2.5 h, 6.5 h, and 18.5 h to inspect the wear tracks. Details are provided in paper B.

Figure 19 shows the Spacer Layer Imaging Method (SLIM) measurements obtained from the ball wear scar at the end of the 18.5-hour test. The SLIM observations confirmed the presence of a physical tribofilm. However, the representation remains largely qualitative, as reliable quantification was not possible due to the extremely thin nature of the tribofilms, likely below 10 nm. Figure 20 illustrates the averaged post-test surface profiles obtained after 6.5 h and 18.5 h of testing. Together, these observations help support the friction trends discussed previously.

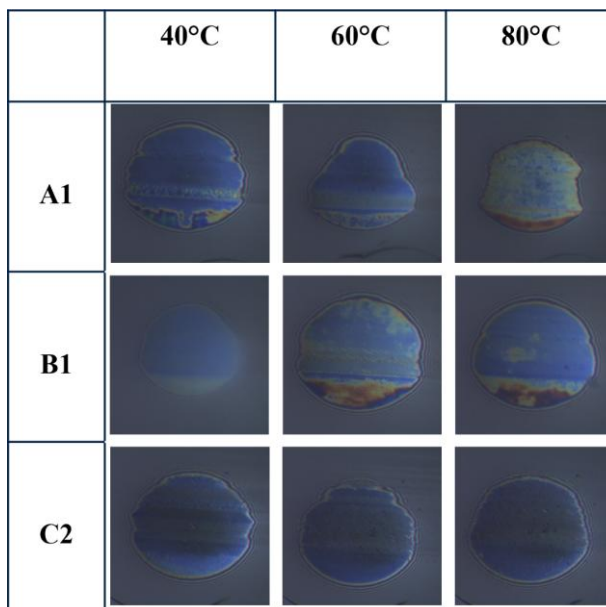


Figure 19: SLIM images of ball wear track recorded at the end of friction tests (18.5 hours) using WBLs at three different temperatures.

At 40 °C, the wear scars produced by the water-based lubricants (WBLs) were comparable to those observed for the reference oil. However, at 60 °C and 80 °C, the wear rates for the WBLs, particularly the glycol-based formulation A1, increased significantly. Fluid A1 exhibited a maximum wear depth of approximately 2500 nm at 60 °C. Paradoxically, the pronounced friction reduction observed for A1 during the later stages of the test may be associated with increased conformity of the contact surfaces resulting from progressive wear.

At 80 °C, the wear depth was lower than that observed at 60 °C, which may indicate the onset of tribofilm formation at elevated temperature. Improved wear performance was observed for B1, with maximum wear depths remaining below 500 nm and showing limited evolution over time. In addition, traces of tribofilm formation were detected for B1 under high-temperature conditions.

The glycerol–water formulation (C2) demonstrated superior surface protection compared with A1 and B1. This behaviour can be attributed primarily to its higher dynamic viscosity (76 mPa·s at 40 °C) and a stronger piezoviscous response, which enhance the hydrodynamic film thickness and reduce asperity interactions. However, no clear evidence of tribofilm formation was observed for C2, suggesting that its performance is governed mainly by bulk rheological properties and hydrodynamic lubrication rather than by the formation of a protective tribofilm layer.

The areal surface topography analysis indicates that sliding and abrasive wear were the dominant mechanisms for the WBLs, with the severity of surface damage increasing with temperature. The glycol-based lubricants (A1 and B1) showed signs of adhesive and abrasive wear, while SEM analysis revealed early-stage spalling. In contrast, the C2 formulation caused comparatively less surface damage. The reference oil exhibited only mild abrasive wear, reflecting its superior film-forming capability and the effectiveness of its additive package. Details can be found in Paper B.

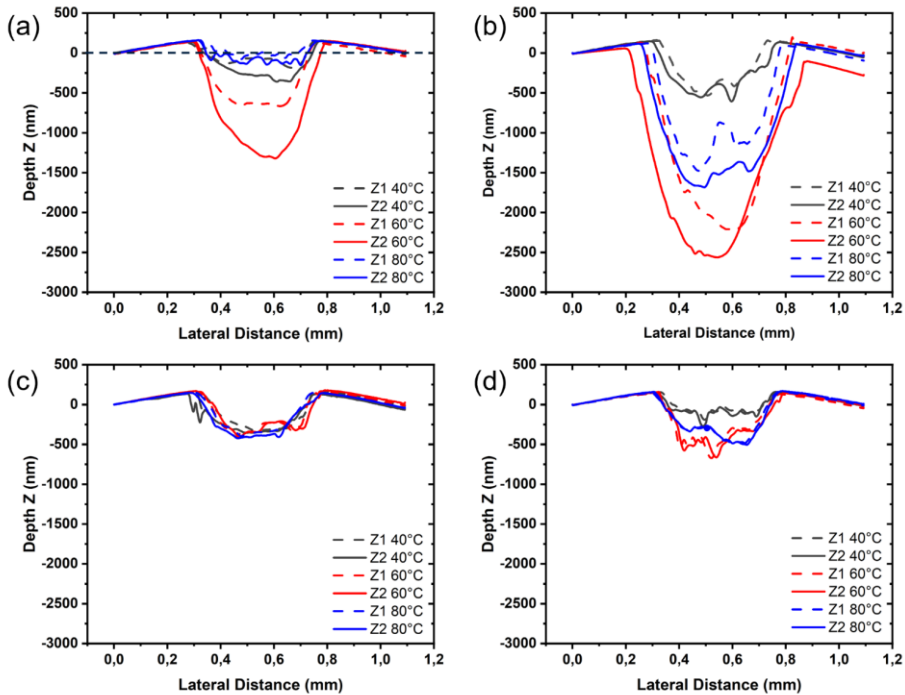


Figure 20: Average wear profiles of the ball wear tracks after 6.5 hours (Z1) and 18.5 hours (Z2), lubricated with (a) reference oil R1, (b) glycol-water A1, (c) glycol-water B1, and (d) glycerol-water C2 solutions.

XPS analysis

X-ray photoelectron spectroscopy (XPS) was performed on wear tracks generated at 60 °C to identify potential additive-derived or tribochemical films. Peak assignments were made in accordance with reference data [116]. The O1s peak at approximately 530.5 eV, observed in all cases, corresponds to iron oxide (Fe_2O_3), indicating surface oxidation of the steel substrate. The C1s peak at 284.8 eV is attributed

to C–C bonds associated with adventitious carbon; its marked reduction after sputter cleaning confirms removal of surface contaminants and residual hydrocarbons.

In the Fe 2p region, peaks at approximately 710–711 eV, 709 eV and 707 eV were assigned to Fe₂O₃, FeO and metallic Fe, respectively, indicating the coexistence of oxidised and unoxidised iron. Following sputtering, a relative shift from Fe₂O₃ to FeO was observed, suggesting removal of superficial layers and exposure of sub-surface oxide. The limited sputter depth implies that only thin surface films were present.

Elemental analysis further revealed Ca 2p peaks at 347.5 eV and 350.5 eV, characteristic of Ca²⁺, and a P 2p peak at approximately 133.5 eV, corresponding to phosphate (PO₄³⁻). A higher binding energy shoulder in the O1s spectrum supports the presence of phosphate species. These findings indicate the formation of a calcium phosphate-containing tribofilm for fluids A1 and B1, with sulphur also detected in these cases. Overall, the results suggest a thin tribochemically formed surface layer composed primarily of iron oxides with contributions from calcium and phosphate species.

5.4 Tribocorrosion behaviour

The presence of water in lubricants can promote electrochemical reactions due to increased ionic conductivity and enhanced surface reactivity when appropriate additives are not present. During sliding, the protective oxide layer on steel may be repeatedly removed by mechanical contact, exposing fresh metal to the electrolyte and accelerating corrosion. This depassivation–repassivation process is characteristic of tribocorrosion systems. Paper D presents the detailed results of this study.

To investigate the coupled interaction between mechanical wear and electrochemical corrosion, tribocorrosion experiments were conducted using a tribometer integrated with an electrochemical cell. The study focused on glycerol-based lubricants, selected for detailed analysis from the previously investigated WBL candidates. Tests were performed on bearing steel under anodic polarisation using three glycerol-based solutions with identical dynamic viscosity and operating conditions.

The first lubricant was a fully formulated aqueous glycerol solution (fluid 1), representative of fluid C2 used in earlier experiments. This fluid showed only minor variations in the potentiostatic signal during sliding. In contrast, the additive-free aqueous glycerol solution (fluid 2) exhibited a pronounced increase in anodic current, indicating significant depassivation and enhanced electrochemical activity.

A non-aqueous glycerol solution (fluid 3) was also examined to isolate the role of water in the tribocorrosion process. In this case, negligible changes in anodic current were observed during sliding, suggesting suppressed electrochemical activity in the absence of water.

Friction and wear behaviour during tribocorrosion test

The tribological results reveal an inverse relationship between friction and wear, despite all fluids having identical viscosity. The observed differences are primarily attributed to variations in interfacial chemistry and lubrication mechanisms.

The aqueous glycerol solutions (fluids 1 and 2) exhibited lower friction coefficients (≈ 0.09 – 0.105). The presence of water modifies interfacial behaviour by promoting the adsorption of water molecules on the metal surface, leading to the formation of hydrated boundary layers. These layers act as low-shear interfacial films, reducing asperity adhesion and consequently lowering friction. However, these aqueous solutions produced higher wear volumes, particularly in the case of unadditivated glycerol aqueous solution. The presence of water increased ionic conductivity and promoted electrochemical reactions, resulting in corrosion-assisted material removal under anodic conditions during sliding.

In contrast, the non-aqueous glycerol solution (fluid 3) showed higher friction (≈ 0.12 – 0.14), likely due to weaker boundary film formation and the absence of hydrated surface layers. Despite the higher friction, this fluid produced the lowest wear volume, as electrochemical degradation was largely suppressed and wear was governed mainly by mechanical processes.

Contribution of chemical wear to overall wear

Chemical wear contributed significantly to the overall material loss in the aqueous systems. In the additive-free glycerol–water solution (Fluid 2), approximately 30% of the total wear volume was attributed to chemical dissolution, estimated from electrochemical charge measurements using Faraday's law.

This contribution arises from tribocorrosion synergy, where mechanical sliding continuously removes the protective oxide layer, exposing fresh metal to the electrolyte. The newly exposed surface undergoes anodic dissolution followed by repassivation, and repeated cycles of film removal and regeneration accelerate material degradation beyond purely mechanical wear. In addition, tribochemical reactions within glycerol–water environments may generate reactive species, including water-derived ions and organic acids, which can increase local conductivity and further promote anodic dissolution within the wear track.

In contrast, the non-aqueous glycerol solution exhibited negligible chemical wear due to limited electrochemical activity, with material removal dominated by mechanical mechanisms such as adhesion and abrasion. Overall, the results highlight the critical role of water content in governing tribocorrosion behaviour through mechanically assisted corrosion processes involving repeated depassivation–repassivation cycles.

5.5 Gearbox drag losses and efficiency

Drag losses represent torque-independent losses generated by lubricant churning, squeezing, and viscous shear within the gearbox. These losses are mainly governed by lubricant density, viscosity, and rotational speed.

At low rotational speed (500 rpm), all water-based lubricants (WBLs) exhibited higher drag losses relative to the reference oil (R1). This behaviour is primarily attributed to the higher density of the WBLs. The effect was most pronounced for C2, whose higher viscosity further increased viscous resistance, see Figure 21.

At higher speeds (6000–10000 rpm), the difference between lubricants decreased, and in some cases, WBLs showed comparable or slightly lower drag losses than the reference oil, see Figure 21(a). This behaviour is likely associated with centrifugal expulsion of lubricant from rotating components, which reduces fluid immersion and limits churning losses. At high temperature the drag losses decrease for all test fluids, however the normalised losses for WBLs remain higher relative to reference oil, Figure 21(b). Overall, drag loss behaviour reflects the competing effects of higher fluid density in WBLs and viscosity-dependent churning resistance, with the relative importance of these mechanisms changing with operating conditions.

Gearbox efficiency reflects the combined contribution of torque-independent losses (drag and churning) and torque-dependent losses from gears and bearings. Across most operating conditions, the glycol-water lubricants A1 and B1 showed higher efficiency than the reference oil, see Figure 22. This improvement is mainly attributed to lower load-dependent losses in rolling/sliding contacts, which result mainly from the lower friction and lower pressure-viscosity response of WBLs.

At low speed (500 rpm), efficiency varied little with torque, indicating that drag losses dominate the total losses in this regime. In contrast, at high speed (6000 rpm), efficiency was lower at small torque values because fixed losses represent a larger fraction of the transmitted power. As torque increases, the relative influence of these fixed losses decreases, leading to improved efficiency.

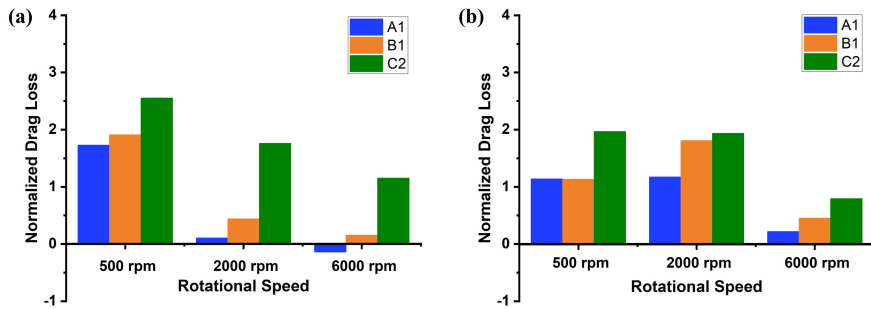


Figure 21: Normalised drag loss (a) at 20 °C (b) at 60 °C for different WBLs with respect to the reference oil (baseline = 0).

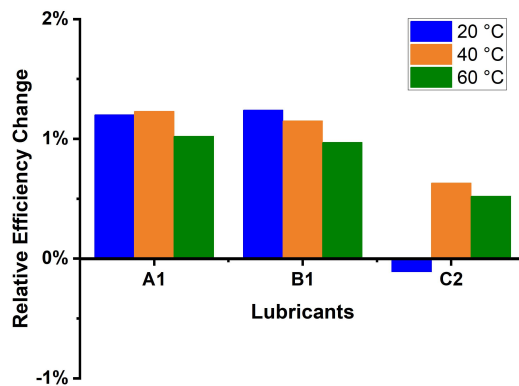


Figure 22: Relative efficiency changes (averaged for 12 test cases for each temperature) for different WBLs with respect to the reference oil (baseline = 0).

Lubricant viscosity strongly influenced efficiency. The high-viscosity fluid C2 showed lower efficiency at low temperature, due to increased viscous drag. In contrast, A1 and B1 provided the best balance between friction reduction and drag losses, resulting in the highest efficiencies.

The temperature rise measured at the rotor bearing provides an indication of frictional heat generation within the gearbox. At 20 °C and 3000 rpm, the reference oil produced the largest temperature increase (~4.8 °C), whereas the WBLs showed significantly lower values (approximately 2.0 °C for A1 and 1.8 °C for B1). At 60 °C and 6000 rpm, the temperature rise increased for all lubricants but remained highest for the reference oil (~7.2 °C). The WBLs again showed lower increases (~2.1 °C for A1 and ~3 °C for B1), while the higher-viscosity fluid C2 showed an intermediate value (~5.1 °C). The reduced temperature rise with WBLs is mainly attributed to lower frictional heat generation in rolling/sliding contacts and the favourable thermal properties of water-containing formulations. Details can be found in Paper C.

Overall, the results demonstrate a clear relationship between drag loss, gearbox efficiency and thermal behaviour. While the higher density of WBLs can increase drag losses at low speeds, their lower friction in lubricated contacts reduces torque-dependent losses, resulting in improved overall efficiency. The reduced frictional heating also leads to lower gearbox temperature rise, highlighting the potential of optimised WBL formulations to improve both energy efficiency and thermal management in drivetrain systems.

5.6 Influence of test setup on WBLs evaporation

The effect of water evaporation on water-based lubricants appears to depend strongly on the experimental configuration. In the tribometer experiments reported in Paper A, the lubricant was tested in a relatively open test chamber, where evaporation could occur more easily during heating. Thermogravimetric analysis showed that evaporation of glycol-water lubricants was minimal (around 1%) at 40 °C but increased significantly at higher temperatures, with approximately 23.5% mass loss at 80 °C. This indicates substantial water evaporation under elevated temperature conditions. Such evaporation alters the effective lubricant composition and can increase viscosity, which may explain the unexpected observation of higher EHL film thickness at elevated temperatures for some WBLs, despite the general expectation that viscosity decreases with increasing temperature.

In contrast, the gearbox experiments described in Paper C were conducted in a closed lubrication circuit with temperatures ranging from 0 °C to 60 °C. In this setup, the lubricant circulated through a reservoir, filter, and heat exchanger, which limited evaporation. Post-test thermogravimetric analysis showed only minor changes in water content, even after long-duration drag loss and efficiency tests, indicating that some evaporation occurred but was not severe enough to significantly destabilise the formulation. Furthermore, post-test characterisation revealed no evidence of degradation or oxidation of the WBLs.

These observations suggest that evaporation effects may be exaggerated in open tribometer studies. In contrast, in practical drivetrain systems with closed lubrication

circuits and heat exchangers, the lubricant composition remains more stable, enabling WBLs to maintain their frictional and thermal advantages.

6 Concluding Remarks

Some concluding remarks are presented here based on the research question stated earlier:

1. Under what operating conditions do water-based lubricants approach superlubricity in engineering surfaces, and how does their friction behaviour vary across lubrication regimes?

- Water-based lubricants consistently produced much lower friction than the reference gear oil across all regimes. Fluid A1 achieved up to 85% friction reduction in full-film lubrication at 40 °C, even at high SRR.
- Superlubricity is achievable by WBLs on engineering steel surfaces at moderate to high entrainment speed, unlike the reference oil. However, the critical speed to achieve superlubricity is strongly dependent on the combination of parameters: water content, viscosity, pressure-viscosity coefficient and surface roughness.
- In boundary and mixed regimes, the friction coefficient of gear oil shows strong temperature dependency due to additive activation at high temperatures. However, WBLs CoF has a weaker temperature dependence due to poor additive activation compared to the reference oil.
- Traction curves for WBLs show low shear behaviour, and unlike conventional oils, they show minimal shear-heating effects and no thermal region is observed.

2. Long-duration test performance and wear mechanisms

- During long-duration rolling/sliding tests, WBLs maintained lower friction than the reference oil. However, WBLs generally produced higher wear, mainly mild abrasive wear with occasional adhesive wear and spalling at elevated temperatures, although wear levels at 40 °C were comparable to gear oil.

- Surface analysis revealed thin tribofilms containing calcium phosphate and sulphur species, indicating additive–surface interaction.
- Long-duration tests were conducted under constant operating conditions. Due to the lower pressure–viscosity coefficient, WBLs formed thinner lubricant films and therefore experienced more severe contact at elevated temperatures (60 °C, 80 °C) than the reference oil. In addition, the additives were not sufficiently effective in providing surface protection under boundary lubrication conditions, which ultimately resulted in increased wear.

3. EHL film formation by WBLs and applicability of classical models

- WBLs can generate sufficient EHL film thickness, enabling surface separation in non-conformal contacts.
- Film thickness is highly sensitive to entrainment speed, SRR, temperature, and composition, and in some cases increases at higher temperatures due to water evaporation and viscosity rise.
- Classical EHL predictions (Hamrock–Dowson) may underestimate or misrepresent film formation in aqueous lubrication systems. WBLs typically operate in the isoviscous–elastic regime with weak pressure–viscosity response, outside the conditions for which the model was developed.

4. Pressure–viscosity behaviour of WBLs

- The key rheological feature of WBLs is very low piezoviscosity, with pressure–viscosity coefficients roughly one order of magnitude lower than PAO oils. Higher water content further reduces this response.
- Pure glycols and glycerol show much stronger pressure–viscosity behaviour than their aqueous formulations and are also more temperature-sensitive.
- Film-thickness-based measurements tend to underestimate pressure–viscosity coefficients for WBLs compared with viscometer measurements, particularly for fluids with extremely weak piezoviscosity.

5. Can water-based lubricants improve gearbox efficiency through reduced friction losses, or do increased water density and associated drag losses offset these benefits?

- At low temperatures, WBLs show higher drag losses due to their higher density.

- However, in most operating conditions friction reduction outweighs drag penalties, and WBLs (especially A1 and B1) achieve higher overall gearbox efficiency than the reference oil.
- Excessively viscous WBLs (e.g., C2) can reduce efficiency due to viscosity-driven churning, particularly at low temperature and low torque.
- WBLs also show thermal advantages, producing significantly lower temperature rise due to reduced frictional heating and improved cooling capacity.

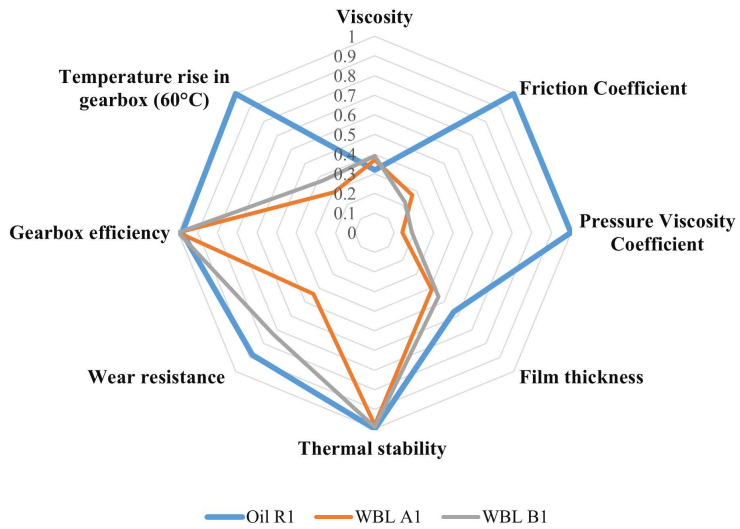
6. Does the presence of water promote tribocorrosion or chemically driven wear, and can additive systems mitigate this degradation?

- The presence of water shifts wear mechanisms toward tribocorrosion, increasing total material loss even when friction remains low.
- The non-additivated aqueous fluid showed the highest wear, with ~30% attributed to chemical wear from wear–corrosion synergy during sliding.
- Additive packages reduced electrochemical activity and chemical wear, demonstrating their protective role.
- Removing water from the test solution eliminated tribocorrosion but increased friction, highlighting the trade-off between low friction and corrosion-driven degradation in aqueous lubrication.

Based on the project outcomes, a holistic comparison between the reference gear oil and the WBLs is presented in Figure 23. The results highlight several performance advantages of the WBL formulations at 40 °C.

Figure 23(a) shows the comparison between the reference oil R1 and the glycol–water lubricants, WBL A1 and WBL B1. Both WBL formulations have viscosity levels comparable to R1; however, they exhibit significantly lower friction coefficients and lower pressure–viscosity coefficients. Despite the lower pressure–viscosity coefficient, the WBLs are still capable of generating an adequate lubricating film thickness. They also demonstrate good thermal stability, although their wear performance is poorer compared with the reference oil. One of the most notable advantages is the increase in gearbox efficiency (1.84 % peak gain and 1.23% averaged for A1). In addition, the temperature rise during gearbox operation at 60 °C is substantially lower (3~4 % gain) for WBLs than that observed with the oil lubricant (11 % gain).

(a)



(b)

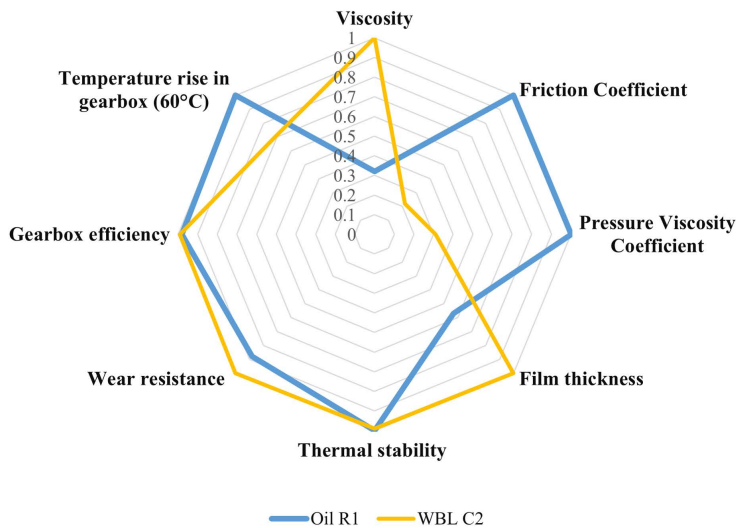


Figure 23: Performance comparison between reference gear oil and WBLs at 40 °C, except for the temperature rise case. (All values are normalised, 1 represents the highest and 0 represents the lowest value).

The comparison between R1 and WBL C2 (glycerol–water) highlights the perspective of the viscosity effect in Figure 23(b). The graph indicates that C2 has significantly higher viscosity, which contributes to greater film thickness even with a relatively low pressure–viscosity coefficient. At 40 °C, C2 exhibits better wear resistance than R1, likely due to enhanced hydrodynamic lubrication. In terms of temperature rise and efficiency, C2 performs slightly better than R1, but its performance is inferior to the other WBL candidates (A1 and B1).

Overall, the WBL lubricants demonstrate an important advantage: lower operating temperatures while maintaining improved gearbox efficiency, which is beneficial for gearbox energy management. Moreover, WBLs specially formulated with glycerol offer a promising sustainability advantage over conventional mineral and synthetic lubricants and provide a more environment friendly lubrication alternative. However, wear remains a significant concern, particularly at elevated temperatures. Therefore, the development of effective additive packages is critical for the successful implementation of WBLs in EV transmission applications.

CHAPTER 7

7 Future Perspectives

Following some future perspectives can be suggested based on the observation of the current study:

Advanced additive formulation for wear mitigation

Paper B shows that although fully formulated WBLs achieve very low friction, reduced film thickness at elevated temperatures increases surface modification and wear, indicating limited durability under boundary and mixed lubrication conditions. Future work should focus on optimising additive packages, such as anti-wear (AW), extreme-pressure (EP), and corrosion inhibitors, to improve tribofilm stability and wear protection.

Mechanistic understanding of WBLs lubrication behaviour

Paper B suggests additive-surface interactions and possible tribofilm formation, while Paper A indicates inlet rheology changes under slide-to-roll ratio (SRR). Further studies using advanced diagnostics, such as infrared (IR) mapping in aqueous EHL contacts, ex-situ ToF-SIMS, and AFM force spectroscopy are needed to better understand surface-sensitive films.

In-situ monitoring of water content in tribological systems

Paper A shows that water evaporation at elevated temperatures can alter viscosity and film formation, whereas water loss is significantly lower in closed systems (Paper C) than in open test chambers (Paper A). Since most measurements are currently performed ex situ, future work should implement in-situ monitoring and control of water content in test systems.

Rolling/sliding tribocorrosion testing for WBL applications

Paper D demonstrates tribocorrosion effects in glycerol-water systems under sliding conditions. Future research should develop rolling/sliding tribocorrosion protocols

representative of gears and bearings and evaluate the behaviour of both conventional bearing steels and corrosion-resistant alloys in WBL environments.

Gearbox lubrication system optimisation for WBLs

Paper C reports that some tests were aborted due to insufficient pumping of high-viscosity fluids under cold conditions, as the gearbox was originally designed for conventional oils. Future studies should therefore address lubrication circuit modification, pumpability, flow management, and evaporation control through design optimisation to ensure reliable WBL operation.

Electrical and material compatibility of WBLs in EV applications

Future work should evaluate dielectric strength, electrical conductivity, and electrochemical behaviour of WBLs as functions of water content, temperature, and ageing. The influence of electric fields or stray currents on material degradation should also be investigated, together with seal and material compatibility for long-term reliability.

REFERENCES

- [1] Mang Theo, Dresel Wilfried. *Lubricants and Lubrication* 2007:894.
- [2] Gohar R. *Elastohydrodynamics*, 2nd Edition 2001:446.
- [3] Rahman MH, Warneke H, Webbert H, Rodriguez J, Austin E, Tokunaga K, et al. *Water-Based Lubricants: Development, Properties, and Performances*. *Lubricants* 2021, Vol 9, 2021;9. <https://doi.org/10.3390/LUBRICANTS9080073>.
- [4] Schmid-Amelunxen M, Schweigkofler M, Kilhau T, Muehlemeier J. *Water-based lubricants* . US8809243B2, 2010.
- [5] Sagraloff N, Dobler A, Tobie T, Stahl K, Ostrowski J. *Development of an Oil Free Water-Based Lubricant for Gear Applications*. *Lubricants* 2019, Vol 7, Page 33 2019;7:33. <https://doi.org/10.3390/LUBRICANTS7040033>.
- [6] Tamayo JGZ, Björling M, Shi Y, Prakash B, Larsson R. *Micropitting performance of glycerol-based lubricants under rolling-sliding contact conditions*. *Tribol Int* 2022;167:107348. <https://doi.org/10.1016/j.triboint.2021.107348>.
- [7] Stadtfeld HJ. *Introduction to Electric Vehicle Transmissions Transmissions in Automobiles with Internal Combustion Engines*. *GEAR TECHNOLOGY* 2020.
- [8] MacHado F, Kollmeyer P, Barroso D, Emadi A. *Multi-Speed Gearboxes for Battery Electric Vehicles: Current Status and Future Trends*. *IEEE Open Journal of Vehicular Technology* 2021;2:419–35. <https://doi.org/10.1109/OJVT.2021.3124411>.
- [9] Flodin A, Kianian B. *Tesla teardown: Identifying potential uses for PM in electric vehicle transmissions*. *Powder Metallurgy Review*, 2021.
- [10] Larsson R. *EHL Film Thickness Behavior*. *Encyclopedia of Tribology* 2013:817–27. https://doi.org/10.1007/978-0-387-92897-5_639/FIGURES/53.
- [11] Larsson R. *Point Contact EHL*. *Encyclopedia of Tribology* 2013:2549–50. https://doi.org/10.1007/978-0-387-92897-5_627/FIGURES/1632.
- [12] Jacobson B. *Rheology and elastohydrodynamic lubrication*. vol. Vol. 19. Elsevier; 1991.
- [13] Bair S. *High Pressure Rheology for Quantitative Elastohydrodynamics*. *High Pressure Rheology for Quantitative Elastohydrodynamics* 2019:1–388. <https://doi.org/10.1016/C2017-0-03927-7>.
- [14] Barus C. *Isothermals, isopiestic and isometrics relative to viscosity*. *Am J Sci* 1893;s3-45:87–96. <https://doi.org/10.2475/ajs.s3-45.266.87>.
- [15] *Chapter 6 Models for the temperature and pressure dependence of low-shear viscosity*. *Tribology and Interface Engineering Series* 2007;54:101–32. [https://doi.org/10.1016/S0167-8922\(07\)80011-3](https://doi.org/10.1016/S0167-8922(07)80011-3).
- [16] Bridgman PW. *The effect of pressure on the viscosity of forty-three pure liquids*. *American Academy of Arts and Sciences* 1926.

- [17] Roelands CJA, Vlugter JC, Waterman HI. The Viscosity-Temperature-Pressure Relationship of Lubricating Oils and Its Correlation With Chemical Constitution. *Journal of Basic Engineering* 1963;85:601–7. <https://doi.org/10.1115/1.3656919>.
- [18] Roelands CJA, Winer WO, Wright WA. Correlational Aspects of the Viscosity-Temperature-Pressure Relationship of Lubricating Oils(Dr In dissertation at Technical University of Delft, 1966). *Journal of Lubrication Technology* 1966;93:209–10. <https://doi.org/10.1115/1.3451519>.
- [19] Blok H. Inverse problem in hydrodynamic lubrication and design directives for lubricated flexible surfaces 1963.
- [20] Doolittle AK. Studies in Newtonian Flow. II. The Dependence of the Viscosity of Liquids on Free-Space. *J Appl Phys* 1951;22:1471–5. <https://doi.org/10.1063/1.1699894>.
- [21] Cohen MH, Turnbull D. Molecular Transport in Liquids and Glasses. *J Chem Phys* 1959;31:1164–9. <https://doi.org/10.1063/1.1730566>.
- [22] Bair S, Mary C, Bouscharain N, Vergne P. An improved Yasutomi correlation for viscosity at high pressure. *Proceedings of the Institution of Mechanical Engineers, Part J: Journal of Engineering Tribology* 2013;227:1056–60. <https://doi.org/10.1177/1350650112474394>.
- [23] Venner CH, Bos J. Effects of lubricant compressibility on the film thickness in EHL line and circular contacts. *Wear* 1994;173:151–65. [https://doi.org/10.1016/0043-1648\(94\)90268-2](https://doi.org/10.1016/0043-1648(94)90268-2).
- [24] Lubrecht AA. The numerical solution of the elastohydrodynamically lubricated line- and point contact problem, using multigrid techniques 1987. <https://doi.org/10.3990/1.9789090015835>.
- [25] E-34 Propulsion Lubricants Committee. Pressure-Viscosity Coefficient Measurement, SAE International, ARP6157A, 2020. <https://doi.org/https://doi.org/10.4271/ARP6157A>.
- [26] Van Leeuwen H. The determination of the pressure-viscosity coefficient of a lubricant through an accurate film thickness formula and accurate film thickness measurements. *Proceedings of the Institution of Mechanical Engineers, Part J: Journal of Engineering Tribology* 2009;223:1143–63. <https://doi.org/10.1243/13506501JET504>.
- [27] Bair S, Qureshi F, Batr S. Accurate Measurements of Pressure-Viscosity Behavior in Lubricants. *TRIBOLOGY TRANSACTIONS* 2002;45:390–6. <https://doi.org/10.1080/10402000208982564>.
- [28] Mia S, Ohno N. Prediction of pressure-viscosity coefficient of lubricating oils based on sound velocity. *Lubrication Science* 2009;21:343–54. <https://doi.org/10.1002/LS.96>.
- [29] Bair S. A critical evaluation of film thickness-derived pressure-viscosity coefficients. *Lubrication Science* 2015;27:337–46. <https://doi.org/10.1002/LS.1284>.
- [30] Bair S. Pressure-viscosity response in the inlet zone for quantitative elastohydrodynamics. *Tribol Int* 2016;97:272–7. <https://doi.org/10.1016/J.TRIBOINT.2016.01.037>.
- [31] Hannon WM, Hager CH, Sadinski RJ. A Comparison of the High-Pressure Viscometry and Optical Inference Methods Used to Determine the Pressure-Viscosity Coefficient. *J Tribol* 2023;145. <https://doi.org/10.1115/1.4056283/1150886>.

- [32] Bair S. A Routine High-Pressure Viscometer for Accurate Measurements to 1 GPa. *Tribology Transactions* 2004;47:356–60. <https://doi.org/10.1080/05698190490455582>.
- [33] Bair S, Liu Y, Wang QJ. The Pressure-Viscosity Coefficient for Newtonian EHL Film Thickness With General Piezoviscous Response. *J Tribol* 2006;128:624–31. <https://doi.org/10.1115/1.2197846>.
- [34] Bair S, Liu Y, Wang QJ. The Pressure-Viscosity Coefficient for Newtonian EHL Film Thickness With General Piezoviscous Response. *J Tribol* 2006;128:624–31. <https://doi.org/10.1115/1.2197846>.
- [35] Bair S. The unresolved definition of the pressure-viscosity coefficient. *Scientific Reports* 2022 12:1 2022;12:3422-. <https://doi.org/10.1038/s41598-022-07470-3>.
- [36] Hamrock BJ, Dowson D. Isothermal Elastohydrodynamic Lubrication of Point Contacts: Part III—Fully Flooded Results. *Journal of Lubrication Technology* 1977;99:264–75. <https://doi.org/10.1115/1.3453074>.
- [37] Hamrock BJ, Dowson D. Isothermal Elastohydrodynamic Lubrication of Point Contacts: Part 1—Theoretical Formulation. *Journal of Lubrication Technology* 1976;98:223–8. <https://doi.org/10.1115/1.3452801>.
- [38] Evans HP, Snidle RW. The Isothermal Elastohydrodynamic Lubrication of Spheres. *Journal of Lubrication Technology* 1981;103:547–57. <https://doi.org/10.1115/1.3251734>.
- [39] Chittenden RJ, Dowson D, Dunn JF, Taylor CM. A theoretical analysis of the isothermal elastohydrodynamic lubrication of concentrated contacts. I. Direction of lubricant entrainment coincident with the major axis of the Hertzian contact ellipse. *Proceedings of the Royal Society of London A Mathematical and Physical Sciences* 1985;397:245–69. <https://doi.org/10.1098/rspa.1985.0014>.
- [40] Nijenbanning G, Venner CH, Moes H. Film thickness in elastohydrodynamically lubricated elliptic contacts. vol. 176. 1994. [https://doi.org/https://doi.org/10.1016/0043-1648\(94\)90150-3](https://doi.org/https://doi.org/10.1016/0043-1648(94)90150-3).
- [41] Hamrock BJ, Dowson D. Minimum film thickness in elliptical contacts for different regimes of fluid-film lubrication. Cleveland, Ohio: 1978.
- [42] Esfahanian M, Hamrock BJ. Fluid-Film Lubrication Regimes Revisited. *Tribology Transactions* 1991;34:628–32. <https://doi.org/10.1080/10402009108982081>.
- [43] Björling M. Friction in Elastohydrodynamic Lubrication Marcus Björling Friction in Elastohydrodynamic Lubrication. Luleå University of Technology, 2014.
- [44] Hasan M, Björling M, Elo R, Matta C, Jantel U, Larsson R. Friction and wear behaviour of fully formulated water-based lubricants under rolling/sliding contacts. *Tribol Int* 2026;217:111669. <https://doi.org/10.1016/j.triboint.2026.111669>.
- [45] Hirano M, Shinjo K. Atomistic locking and friction. *Phys Rev B* 1990;41:11837–51. <https://doi.org/10.1103/PhysRevB.41.11837>.
- [46] Björling M, Shi Y. DLC and Glycerol: Superlubricity in Rolling/Sliding Elastohydrodynamic Lubrication. *Tribol Lett* 2019;67. <https://doi.org/10.1007/s11249-019-1135-1>.
- [47] Han T, Zhang S, Zhang C. Unlocking the secrets behind liquid superlubricity: A state-of-the-art review on phenomena and mechanisms. *Friction* 2021 10:8 2022;10:1137–65. <https://doi.org/10.1007/S40544-021-0586-1>.
- [48] Hofmann S, Björling M, Larsson R, Lohner T, Stahl K. A comment on the review paper “Critical advances in superlubricity: From current challenges to sustainable

- development beyond laboratory” from a gear perspective. *Friction* 2025. <https://doi.org/10.26599/frict.2025.9441208>.
- [49] Raviv U, Klein J. Fluidity of Bound Hydration Layers. *Science* (1979) 2002;297:1540–3. <https://doi.org/10.1126/science.1074481>.
- [50] Perkin S, Goldberg R, Chai L, Kampf N, Klein J. Dynamic properties of confined hydration layers. *Faraday Discuss* 2009;141:399–413. <https://doi.org/10.1039/B805244A>.
- [51] Han T, Zhang C, Li J, Yuan S, Chen X, Zhang J, et al. Origins of Superlubricity Promoted by Hydrated Multivalent Ions. *J Phys Chem Lett* 2020;11:184–90. <https://doi.org/10.1021/ACS.JPCLETT.9B03098>.
- [52] Zhang S, Zhang C, Hu Y, Ma L. Numerical simulation of mixed lubrication considering surface forces. *Tribol Int* 2019;140:105878. <https://doi.org/10.1016/j.triboint.2019.105878>.
- [53] Deng M, Li J, Zhang C, Ren J, Zhou N, Luo J. Investigation of running-in process in water-based lubrication aimed at achieving super-low friction. *Tribol Int* 2016;102:257–64. <https://doi.org/10.1016/j.triboint.2016.05.023>.
- [54] Zhang S, Zhang C, Chen X, Li K, Jiang J, Yuan C, et al. XPS and ToF-SIMS analysis of the tribochemical absorbed films on steel surfaces lubricated with diketone. *Tribol Int* 2019;130:184–90. <https://doi.org/10.1016/j.triboint.2018.09.018>.
- [55] Li K, Amann T, Walter M, Moseler M, Kailer A, Rühle J. Ultralow Friction Induced by Tribochemical Reactions: A Novel Mechanism of Lubrication on Steel Surfaces. *Langmuir* 2013;29:5207–13. <https://doi.org/10.1021/la400333d>.
- [56] Ge X, Halmans T, Li J, Luo J. Molecular behaviors in thin film lubrication—Part three: Superlubricity attained by polar and nonpolar molecules. *Friction* 2019;7:625–36. <https://doi.org/10.1007/s40544-018-0254-2>.
- [57] He F, Xie G, Luo J. Electrical bearing failures in electric vehicles. *Friction* 2020;8:4–28. <https://doi.org/10.1007/s40544-019-0356-5>.
- [58] Zhu J, Kim H, Chen H, Erickson R, Maksimovic D. High efficiency SiC traction inverter for electric vehicle applications. *Conference Proceedings - IEEE Applied Power Electronics Conference and Exposition - APEC 2018;2018-March:1428–33*. <https://doi.org/10.1109/APEC.2018.8341204>.
- [59] Busse D, Erdman J, Kerkman RJ, Schlegel D, Skibinski G. Bearing currents and their relationship to PWM drives. *IEEE Trans Power Electron* 1997;12:243–52. <https://doi.org/10.1109/63.558735>.
- [60] Shore JF, Christodoulas AI, Kolekar AS, Lockwood FE, Kadirci A. Prediction of Electric Vehicle Transmission Efficiency Using a New Thermally Coupled Lubrication Model, 2022. <https://doi.org/10.4271/2022-01-5026>.
- [61] Michaelis K, Höhn B-R, Hinterstoiber M. Influence factors on gearbox power loss. *Industrial Lubrication and Tribology* 2011;63:46–55. <https://doi.org/10.1108/00368791111101830>.
- [62] Motin A, Ganamet A. Electric Vehicle Drive Unit Power Losses and Efficiency Estimation: A Coupled 1D Analytical and 3D CFD Approach for High Fidelity Prediction, 2025. <https://doi.org/10.4271/2025-01-8522>.
- [63] Changenet C, Vexel P. Housing influence on churning losses in geared transmissions. *Journal of Mechanical Design* 2008;130:0626031–6. <https://doi.org/10.1115/1.2900714/470496>.

- [64] Shore JF, Kolekar AS, Ren N, Kadiric A. An Investigation Into the Influence of Viscosity on Gear Churning Losses by Considering the Effective Immersion Depth. *Tribology Transactions* 2023;66:906–19. <https://doi.org/10.1080/10402004.2023.2247041>;WGROU:STRING:PUBLICATION.
- [65] Kolekar AS, Olver A V., Sworski AE, Lockwood FE. Windage and churning effects in dipped lubrication. *J Tribol* 2014;136. <https://doi.org/10.1115/1.4025992/377815>.
- [66] Leprince G, Changenet C, Ville F, Vex P, Dufau C, Jarnias F. Influence of aerated lubricants on gear churning losses—an engineering model. *Tribology Transactions* 2011;54:929–38. <https://doi.org/10.1080/10402004.2011.597542>;WEBSITE:WEBSITE:TFOPB;PAGEGROUP:STRING:PUBLICATION.
- [67] Rudston SG, Whitby RD. Recent developments in the performance properties of water based cutting and hydraulic fluids. *Journal of Synthetic Lubrication* 1985;2:183–212. <https://doi.org/10.1002/jsl.3000020302>.
- [68] Spikes HA. Wear and fatigue problems in connection with water-based hydraulic fluids. *Journal of Synthetic Lubrication* 1987;4:115–35. <https://doi.org/10.1002/jsl.3000040203>.
- [69] Ratoi-Salagean M, Spikes H. The Lubricant Film-Forming Properties of Modern Fire Resistant Hydraulic Fluids. *Tribology of Hydraulic Pump Testing*, ASTM International 100 Barr Harbor Drive, PO Box C700, West Conshohocken, PA 19428-2959; 1997, p. 21–37. <https://doi.org/10.1520/STP11833S>.
- [70] El Bahi H, Raisin J, Latchou A, Chaminand J, Cao Y, Yang L. Water-based Lubricant as a new pathway for Electric Vehicle Lubrication. *CTI SYMPOSIUM “Automotive Drivetrain, Intelligent, Electrified”* Berlin, 2022.
- [71] Schmid-Amelunxen M, Schweigkofler M, Kiltbau T, Muehlemeier J. Water-based lubricants. US8809243B2. U.S. Patent and Trademark Office. US8809243B2, 2014.
- [72] Kano M. Super low friction of DLC applied to engine cam follower lubricated with ester-containing oil. *Tribol Int* 2006;39:1682–5. <https://doi.org/10.1016/j.triboint.2006.02.068>.
- [73] Kano M, Yasuda Y, Okamoto Y, Mabuchi Y, Hamada T, Ueno T, et al. Ultralow friction of DLC in presence of glycerol mono-oleate (GMO). *Tribol Lett* 2005;18:245–51. <https://doi.org/10.1007/s11249-004-2749-4>.
- [74] De Barros Bouchet MI, Matta C, Le-Mogne Th, Michel Martin J, Sagawa T, Okuda S, et al. Improved mixed and boundary lubrication with glycerol-diamond technology. *Tribology - Materials, Surfaces & Interfaces* 2007;1:28–32. <https://doi.org/10.1179/175158407x181507>.
- [75] Bouchet MIDB, Matta C, Le-Mogne T, Martin JM, Zhang Q, Goddard W, et al. Superlubricity mechanism of diamond-like carbon with glycerol. Coupling of experimental and simulation studies. *J Phys Conf Ser* 2007;89:012003. <https://doi.org/10.1088/1742-6596/89/1/012003>.
- [76] Joly-Pottuz L, Martin JM, De Barros Bouchet MI, Belin M. Anomalous low friction under boundary lubrication of steel surfaces by polyols. *Tribol Lett* 2009;34:21–9. <https://doi.org/10.1007/s11249-008-9377-3>.

- [77] Habchi W, Matta C, Joly-Pottuz L, De Barros MI, Martin JM, Vergne P. Full film, boundary lubrication and tribochemistry in steel circular contacts lubricated with glycerol. *Tribol Lett* 2011;42:351–8. <https://doi.org/10.1007/S11249-011-9778-6>.
- [78] Matta C, Joly-Pottuz L, De Barros Bouchet MI, Martin JM, Kano M, Zhang Q, et al. Superlubricity and tribochemistry of polyhydric alcohols. *Phys Rev B Condens Matter Mater Phys* 2008;78. <https://doi.org/10.1103/PhysRevB.78.085436>.
- [79] Nacini VF, Björling M, Larsson JA, Larsson R. Tribochemistry of glycerol–water mixtures confined between ferrous substrates: An atomic-scale concept by reactive molecular dynamics simulation. *Tribol Int* 2025;202:110322. <https://doi.org/10.1016/j.triboint.2024.110322>.
- [80] Shi Y, Minami I, Grahn M, Björling M, Larsson R. Boundary and elastohydrodynamic lubrication studies of glycerol aqueous solutions as green lubricants. *Tribol Int* 2014;69:39–45. <https://doi.org/10.1016/J.TRIBOINT.2013.08.013>.
- [81] Li J, Zhang C, Luo J. Superlubricity behavior with phosphoric acid–water network induced by rubbing. *Langmuir* 2011;27:9413–7. <https://doi.org/10.1021/la201535x>.
- [82] Li J, Zhang C, Luo J. Superlubricity achieved with mixtures of polyhydroxy alcohols and acids. *Langmuir* 2013;29:5239–45. <https://doi.org/10.1021/la400810c>.
- [83] Chen Z, Liu Y, Zhang S, Luo J. Controllable superlubricity of glycerol solution via environment humidity. *Langmuir* 2013;29:11924–30. <https://doi.org/10.1021/la402422h>.
- [84] Long Y, Bouchet MDB, Lubrecht T, Onodera T, Martin JM. Superlubricity of glycerol by self-sustained chemical polishing 2019:1–13. <https://doi.org/10.1038/s41598-019-42730-9>.
- [85] Ma Q, He T, Khan AM, Wang Q, Chung YW. Achieving macroscale liquid superlubricity using glycerol aqueous solutions. *Tribol Int* 2021;160:107006. <https://doi.org/10.1016/j.triboint.2021.107006>.
- [86] Ma Q, Wang W, Dong G. Achieving Macroscale Liquid Superlubricity Using Lubricant Mixtures of Glycerol and Propanediol. *Tribol Lett* 2021;69:159. <https://doi.org/10.1007/s11249-021-01519-6>.
- [87] Hua J, Björling M, Larsson R, Shi Y. Controllable superlubricity achieved with mixtures of green ionic liquid and glycerol aqueous solution via humidity. *J Mol Liq* 2022;345. <https://doi.org/10.1016/j.molliq.2021.117860>.
- [88] Ma Q, Liang M, Xu X, Yan C, Wang H. Towards direct superlubricity and negligible wear with polyalcohol lubricant mixtures of ethylene glycol and glycerol for steel tribopairs. *Appl Surf Sci* 2024;663:160151. <https://doi.org/10.1016/j.apsusc.2024.160151>.
- [89] Li L, Gong P, Bai P, Wen X, Meng Y, Ding J, et al. Impact of Water Content on the Superlubricity of Ethylene Glycol Solutions. *Lubricants* 2023;11:466. <https://doi.org/10.3390/lubricants11110466>.
- [90] Poláček T, Šperka P, Křupka I. Liquid superlubricity of lubricants containing hydroxyl groups and their aqueous solution under rolling/sliding conditions. *Friction* 2024;12:164–73. <https://doi.org/10.1007/S40544-023-0762-6/METRICS>.

- [91] Yilmaz M, Mirza M, Lohner T, Stahl K. Superlubricity in EHL Contacts with Water-Containing Gear Fluids. *Lubricants* 2019, Vol 7, Page 46 2019;7:46. <https://doi.org/10.3390/LUBRICANTS7050046>.
- [92] Yilmaz M, Lohner T, Michaelis K, Stahl K. Minimizing gear friction with water-containing gear fluids. *Forsch Ingenieurwes* 2019;83:327–37. <https://doi.org/10.1007/s10010-019-00373-2>.
- [93] Hofmann S, Lohner T, Stahl K. Influence of water content on elastohydrodynamic friction and film thickness of water-containing polyalkylene glycols. *Front Mech Eng* 2023;9:1128447. <https://doi.org/10.3389/FMECH.2023.1128447/BIBTEX>.
- [94] Biresaw G, Bantchev GB. Pressure viscosity coefficient of vegetable oils. *Tribol Lett* 2013;49:501–12. <https://doi.org/10.1007/S11249-012-0091-9/TABLES/5>.
- [95] Zhang CH, Zhao YC, Björling M, Wang Y, Luo J Bin, Prakash B. EHL properties of polyalkylene glycols and their aqueous solutions. *Tribol Lett* 2012;45:379–85. <https://doi.org/10.1007/S11249-011-9883-6/FIGURES/8>.
- [96] Asada K, Cayer-Barrioz J, Mazuyer D. Elastohydrodynamic Film Formation and Sol/Gel Transition of Aqueous Fluids. *Tribol Lett* 2022;70:1–10. <https://doi.org/10.1007/S11249-022-01640-0/FIGURES/9>.
- [97] Mungroo A, Mazuyer D, Cayer-Barrioz J. Thin Film-Formation Mechanisms of Aqueous Lubricant in Elastohydrodynamic Lubrication. *Tribology Letters* 2025 73:2 2025;73:65-. <https://doi.org/10.1007/s11249-025-01998-x>.
- [98] Hofmann S, Lohner T, Stahl K. Influence of water evaporation on elastohydrodynamic lubrication with water-containing polyalkylene glycols. *Friction* 2024;12:2370–88. <https://doi.org/10.1007/s40544-024-0916-1>.
- [99] Yilmaz M, Lohner T, Michaelis K, Stahl K. Bearing Power Losses with Water-Containing Gear Fluids. *Lubricants* 2020, Vol 8, Page 5 2020;8:5. <https://doi.org/10.3390/LUBRICANTS8010005>.
- [100] Morhard B, Schwarz B, Pointner-Gabriel L, Lohner T, Stahl K. Efficiency improvement potential of a BEV gearbox using a mono fluid circuit. *Forschung Im Ingenieurwesen* 2025 89:1 2025;89:1–11. <https://doi.org/10.1007/S10010-025-00840-Z>.
- [101] Hofmann S, Lohner T, Stahl K. Influence of water evaporation on the power loss behavior of cylindrical gears lubricated by aqueous polyalkylene glycols. *Forschung Im Ingenieurwesen* 2025 89:1 2025;89:1–19. <https://doi.org/10.1007/S10010-025-00886-Z>.
- [102] Shao S, Zhang K, Yao Y, Liu Y, Jin S, Wang Z. A novel model for investigating the thermal equilibrium characteristics of a high-speed train gearbox. *Alexandria Engineering Journal* 2025;124:319–36. <https://doi.org/10.1016/J.AEJ.2025.03.100>.
- [103] Koffel G, Vile F, Changenet C, Vexlex P. Investigations on the power losses and thermal effects in gear transmissions. *Proceedings of the Institution of Mechanical Engineers, Part J: Journal of Engineering Tribology* 2009;223:469–79. <https://doi.org/10.1243/13506501JET483;ISSUE:ISSUE:DOI>.
- [104] Lehmann R, Petuchow A, Moullion M, Künzler M, Windel C, Gauterin F. Fluid Choice Based on Thermal Model and Performance Testing for Direct Cooled Electric Drive. *Energies* 2020, Vol 13, Page 5867 2020;13:5867. <https://doi.org/10.3390/EN13225867>.

- [105] Huang A, Bao Y, Li H, Liu Y, Zheng X, Qin G. Thermal conductivity of ethylene glycol and water binary mixtures at evaluated temperature and pressure. *J Chem Thermodyn* 2022;175:106900. <https://doi.org/10.1016/J.JCT.2022.106900>.
- [106] Bosch J, DellaCorte C. Rheological Characterization and Tribological Evaluation of Water-Based Lubricants in AISI 52100 Bearing Steel. *Tribol Lett* 2024;72:10. <https://doi.org/10.1007/s11249-023-01811-7>.
- [107] Matta C, Berens F, Kerrigan A, Meeuwenoord R, van der Zwaan R, Prol DA, et al. Influence of emerging E-fluids on rolling/sliding bearing contacts. *Tribol Int* 2025;212:110986. <https://doi.org/10.1016/J.TRIBOINT.2025.110986>.
- [108] Tomala A, Karpinska A, Werner WSM, Olver A, Störi H. Tribological properties of additives for water-based lubricants. *Wear* 2010;269:804–10. <https://doi.org/10.1016/j.wear.2010.08.008>.
- [109] Khanmohammadi H, Wijanarko W, Espallargas N. Ionic Liquids as Additives in Water-Based Lubricants: From Surface Adsorption to Tribofilm Formation. *Tribol Lett* 2020;68:130. <https://doi.org/10.1007/s11249-020-01377-8>.
- [110] Wijanarko W, Khanmohammadi H, Espallargas N. Ionic liquids as boundary additives in water-based and PAO lubricants. *Friction* 2022;10:1405–23. <https://doi.org/10.1007/s40544-021-0550-0>.
- [111] Cousseau T, Björling M, Graça B, Campos A, Seabra J, Larsson R. Film thickness in a ball-on-disc contact lubricated with greases, bleed oils and base oils. *Tribol Int* 2012;53:53–60. <https://doi.org/10.1016/J.TRIBOINT.2012.04.018>.
- [112] Hartl M, Křupka I, Poliščuk R, Liška M. An Automatic System for Real-Time Evaluation of EHD Film Thickness and Shape Based on the Colorimetric Interferometry. *TRIBOLOGY TRANSACTIONS* 1999;42:303–9. <https://doi.org/10.1080/10402009908982221>.
- [113] PCS INSTRUMENTS: MTM 2 Mini-Traction Machine 2013.
- [114] Wakeham WA, Assael MJ, Avelino HMNT, Bair S, Baled HO, Bamgbade BA, et al. In Pursuit of a High-Temperature, High-Pressure, High-Viscosity Standard: The Case of Tris(2-ethylhexyl) Trimellitate. *J Chem Eng Data* 2017;62:2884–95. https://doi.org/10.1021/ACS.JCED.7B00170/SUPPL_FILE/IE7B00170_SI_002.ZIP.
- [115] López-Ortega A, Arana JL, Bayón R. Tribocorrosion of Passive Materials: A Review on Test Procedures and Standards. *International Journal of Corrosion* 2018;2018:1–24. <https://doi.org/10.1155/2018/7345346>.
- [116] Moulder JF, Stickle WF, Sobol PE, Bomben KD. Handbook of X-Ray Photoelectron Spectroscopy (Perkin-Elmer, Eden Prairie, MN, 1992). Google Scholar 2002:128.

Department of Engineering Sciences and Mathematics
Division of Machine Elements

ISSN 1402-1544
ISBN 978-91-8048-995-9 (print)
ISBN 978-91-8048-996-6 (pdf)

Luleå University of Technology 2026